AD-A170 459 OPTICAL ENHANCEMENT OF DEGRADED FINGERPRINTS(U) AIR FORCE INST OF TECH WRIGHT-PATTERSON AFB OH H E OLIMB MAY 86 AFIT/CI/NR-86-95T 1/1

UNCLASSIFIED F/G 20/6 NL

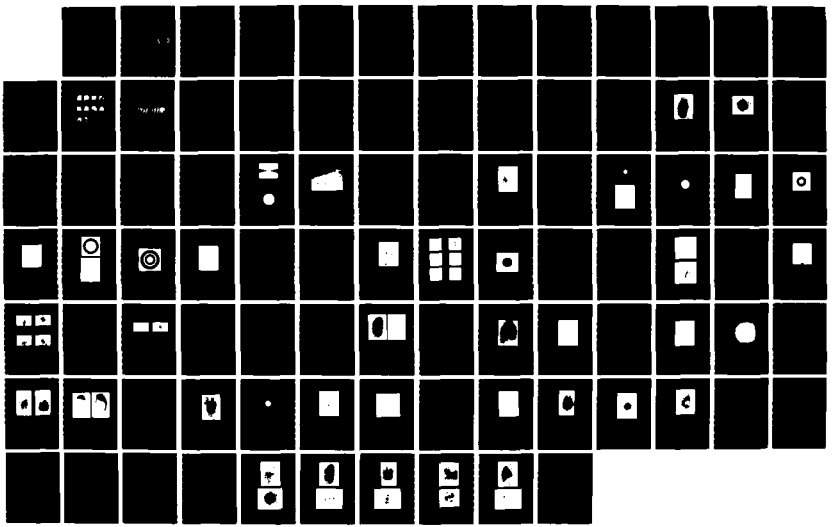

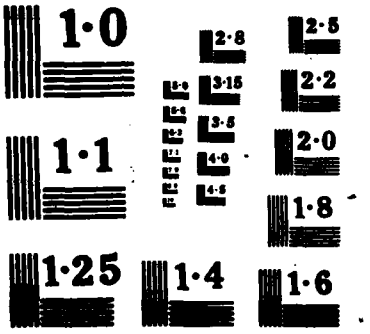
1·0
1·1
1·25
2·8
3·15
3·5
4·0
4·5
1·4
2·5
2·2
2·0
1·8
1·6

SECURITY CLASSIFICATION OF THIS PAGE (When Data Entered)

REPORT DOCUMENTATION PAGE

READ INSTRUCTIONS BEFORE COMPLETING FORM

1. REPORT NUMBER: AFIT/CI/NR 86-95T	2. GOVT ACCESSION NO.
3. RECIPIENT'S CATALOG NUMBER	
4. TITLE (and Subtitle): Optical Enhancement of Degraded Fingerprints	5. TYPE OF REPORT & PERIOD COVERED: THESIS/DISSERTATION
	6. PERFORMING ORG. REPORT NUMBER
7. AUTHOR(s): Hal Erling Olimb	8. CONTRACT OR GRANT NUMBER(s)
PERFORMING ORGANIZATION NAME AND ADDRESS: AFIT STUDENT AT:Texas Tech University	10. PROGRAM ELEMENT, PROJECT, TASK AREA & WORK UNIT NUMBERS
CONTROLLING OFFICE NAME AND ADDRESS: AFIT/NR, WPAFB OH 45433-6583	12. REPORT DATE: 1986
	13. NUMBER OF PAGES: 85
MONITORING AGENCY NAME & ADDRESS(if different from Controlling Office)	15. SECURITY CLASS. (of this report): UNCLAS
	15a. DECLASSIFICATION/DOWNGRADING SCHEDULE

DISTRIBUTION STATEMENT (of this Report)

APPROVED FOR PUBLIC RELEASE; DISTRIBUTION UNLIMITED

DTIC ELECTE AUG 1 2 1986 S D E

17. DISTRIBUTION STATEMENT (of the abstract entered in Block 20, if different from Report)

18. SUPPLEMENTARY NOTES

APPROVED FOR PUBLIC RELEASE: IAW AFR 190-1

LYNN E. WOLAVER 6AUG 86
Dean for Research and
Professional Development
AFIT/NR

19. KEY WORDS (Continue on reverse side if necessary and identify by block number)

20. ABSTRACT (Continue on reverse side if necessary and identify by block number)

ATTACHED.

86 8 11 005

DD FORM 1 JAN 73 1473 EDITION OF 1 NOV 65 IS OBSOLETE

SECURITY CLASSIFICATION OF THIS PAGE (When Data Entered)

AD-A170 459

DTIC FILE COPY

OPTICAL ENHANCEMENT OF DEGRADED FINGERPRINTS

by

HAL ERLING OLIMB, B.S. in E.E.

A THESIS

IN

ELECTRICAL ENGINEERING

Submitted to the Graduate Faculty
of Texas Tech University in
Partial Fulfillment of
the Requirements for
the Degree of

MASTER OF SCIENCE

IN

ELECTRICAL ENGINEERING

Approved

Thomas F. Krile
Chairperson of the Committee

John F. Walkup

Thomas G. Newman

Accepted

Dean of the Graduate School

May, 1986

ACKNOWLEDGEMENTS

I am extremely grateful to Dr. Thomas Krile and Dr. John Walkup for their academic and spiritual support and guidance. I thank my fellow Optical Systems Laboratory students, especially Robert Hobbs and Dave Lojewski, for their friendship and encouragement. I am grateful to Jeannette Davis for her role in preparing and typing this thesis. I appreciate the photography done by Joe Hartley and Bobby Jones and the help of Brent Boren. I gratefully acknowledge the opportunity and support provided by the USAF. Finally, I lovingly thank my wife, Shirley, for her strength and understanding during my graduate program.

ABSTRACT

The similarities and differences between fingerprints enable degraded fingerprints to be optically enhanced for the purpose of identification. A coherent optical processing system was used to locate and analyze the spectra of features that uniquely identify fingerprints. The spectra of these ridges and ridge characteristics (minutiae) are located in harmonic bands of spatial frequencies for all types of fingerprints. A general set of simple filters was developed to enhance the identifying features of degraded fingerprints. Simple binary filters (lowpass, bandpass, highpass, and contrast reversal) use the circular symmetry of fingerprint spectra to enhance the degraded fingerprints. Schlieren and Laplacian filters perform an edge enhancement on the fingerprint ridges. These techniques improved the identifiability of degraded fingerprints while maintaining the generality of the procedure and the integrity of the fingerprints.

TABLE OF CONTENTS

LIST OF FIGURES

CHAPTER I

INTRODUCTION

All fingerprints are unique [1]. The differences between fingerprints are based on the type and position of the ridge characteristics. All fingerprints are also similar. Groups of fingerprints are distinguished by the similarities in the ridge patterns. Thus, fingerprints are identified by their differences and classified by their similarities.

Degraded fingerprints retain these similarities and differences. For example, ridges that are hidden by additive or multiplicative degradations can be recovered [2]. Latent fingerprints (impressions transferred from fingers by touching a surface) are normally incomplete and degraded. Smudged or smeared fingerprints may be distinguishable but not identifiable. The ridge pattern may not be retained, but the characteristic differences remain. In either case, the problem is to develop techniques that enhance latent or degraded fingerprints while maintaining the characteristic differences within like ridge patterns.

Fingerprint enhancement techniques can be implemented using either digital computers or optical processors. Digital computers are inherently serial devices that can enhance images by directly manipulating pixels in the spatial domain or in the spatial frequency domain [3-5]. Since optical systems are inherently parallel

processors, they can enhance images in real time by modifying the Fourier spectra.

Previous fingerprint processing research has concentrated on searching fingerprint files by directly comparing the "good" fingerprints on file with the latent fingerprints or by comparing encoded characteristics. The optical processors use matched filter and pattern recognition techniques. For example, after "good" fingerprint spectra are recorded holographically, latent fingerprints are correlated with the "good" fingerprints using a coherent optical processor [6-7]. Digital fingerprint identification systems rely on high speed optical scanners to digitize the fingerprint images and data processing techniques to match fingerprints stored in partitioned files. The fingerprints are encoded either automatically or with an operator's interactive assistance. The encoding is made according to established fingerprint classification methods. Preprocessing techniques are applied to fill in small breaks in ridges and separate out blurred areas of the fingerprint [8].

Recently digital image enhancement techniques have been applied in an effort to automate latent fingerprint identification [9]. Depending on the specific application, optical enhancement techniques may also be useful. Optical systems are fast and small, but they are not very flexible. This inflexibility may not be important for certain applications [10-11].

The purpose of this research is to investigate using optical image processing techniques to enhance degraded fingerprints.

Coherent optical processing techniques are applied to locate and enhance the essential information in a fingerprint. This will be accomplished by starting at the end and working backwards. First, a "good" fingerprint will be used to locate the spectral information that corresponds to the unique spatial features. Then the fingerprint will be degraded with known degradations. With knowledge of the original fingerprint, the degraded version will be enhanced using spatial filtering techniques. Finally, the enhanced version of the fingerprint will be compared with the original to check for artifact generation [12]. The figure of merit for the enhancement will be the increase in the identifiable ridge information. Throughout this thesis, a latent tented arch type fingerprint (shown in Figure 3-1) will be used as the primary example of a "good" fingerprint.

Ultimately, this research will show that a general set of optical filters can be developed for enhancing degraded fingerprints. The filters will be made general by using the similarities in fingerprint ridge patterns. They will enhance the identifiable differences. Since the filters will actually modify the Fourier spectra of the fingerprints, they rely on the fact that the similarities in the ridge patterns and the differences in the ridge characteristics are maintained (although in a different form) through a Fourier transform.

This chapter contains introductory remarks on fingerprints and past and present automated fingerprint identification systems. It also includes statements concerning the objectives of this thesis in

using optical processing techniques to enhance latent and degraded fingerprints.

In Chapter II the fundamental concepts of fingerprint identification and coherent optical processing are presented to establish a common background. The problems with enhancing and identifying latent or degraded fingerprints are stated.

The integrity of the fingerprints must be maintained. Thus, in Chapter III, the location of the essential, identifying information is established. While investigating the characteristics of the Fourier spectra of fingerprints, spatial filters were generated that are used for enhancing latent and degraded fingerprints.

In Chapter IV, simple filters are used to enhance latent and degraded fingerprints. These simple filters form a set of general filters that are used to enhance various types of fingerprints.

Finally, Chapter V contains concluding statements about the results of locating and enhancing the identifiable features of fingerprints. With this evidence and the results of Chapters III and IV, the possibilty of enhancing a broad class of fingerprints using a general set of filters is discussed.

CHAPTER II

FUNDAMENTALS

In this chapter the ridge characteristics that identify fingerprints are described. Also, the basic principles of coherent optical processing, used for finding and enhancing these characteristics, are presented.

2.1 Fingerprints

Fingerprints are the most practical and reliable means of identification. They are essentially invariant over time; except for growth, the ridge characteristics don't change. Each fingerprint is unique; the intricate ridge patterns are not duplicated in any other fingerprint. They are permanent and nontransferable; fingerprints that are marred (cut or scarred) or absent (ridges that are rubbed off intentionally or by manual labor) are also unique. And they are easily recorded and stored for use in establishing identity.

Fingerprint classification and identification techniques are based on the permanence of fingerprint characteristics and the uniqueness of the ridge detail. These processes are closely related, but they are not identical. In this thesis fingerprint classification will be presented only as it directly relates to fingerprint identification.

2.1.1 Fingerprint Classification

Fingerprints are classified to facilitate the filing, searching, and retrieval of fingerprint records. Initially, the fingerprints are grouped by general and specific ridge patterns. There are three major groups of patterns: arches, loops, and whorls. These groups are subdivided according to the type of pattern. Examples of these pattern types are shown in Figure 2-1. The fingerprints are further grouped by specific pattern details according to an ordered set of rules [13].

These ridge patterns are also the first step in identifying a fingerprint; they limit the scope of the search by identifying a fingerprint's general and/or specific pattern type. The identification of the fingerprint does not require that the pattern type be known; the classification problem does.

2.1.2 Fingerprint Identification

The characteristics that uniquely identify a fingerprint are called minutiae. They consist of all the features, including scars, that appear consistently in a fingerprint. They are the deviations in the ridge pattern. In most fingerprints, these features or deviations are the ridges that join, separate, or end.

There are three basic types of minutiae: bifurcations, ridge endings, and short independent ridges. All ridge characteristics can be described by combining these basic types [14]. Examples of minutiae are shown in Figure 2-2.

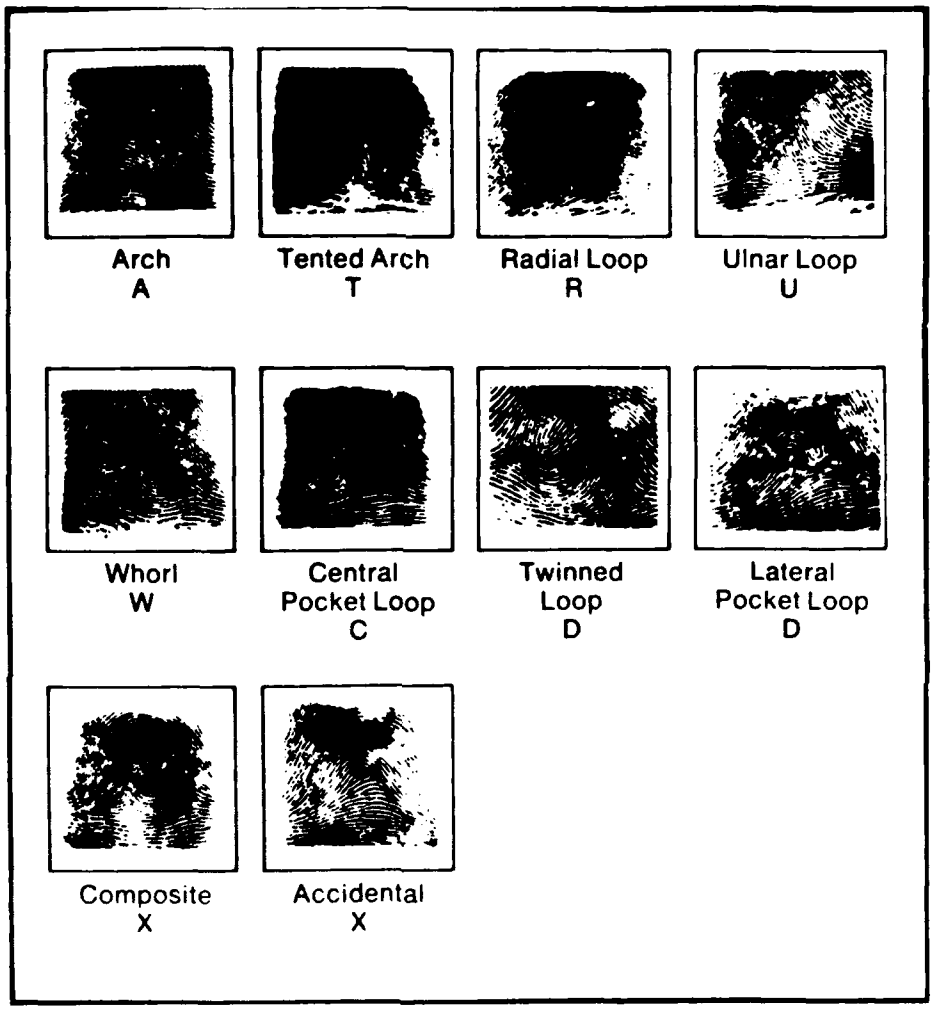

Figure 2-1. General Types of Fingerprint Patterns.

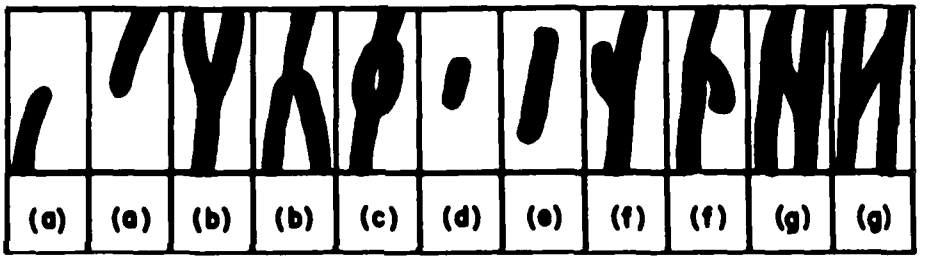

Figure 2-2. Basic Types of Ridge Characteristics Found in Fingerprints.

The identification of fingerprints is based upon the minutiae and their location. This makes it possible to identify incomplete and partially degraded fingerprints. Areas of fingerprints that are wholly degraded may have to be "restored" before they can be identified.

New techniques are being developed for detecting and recording latent fingerprints [15-16]. These techniques locate fingerprints that conventional techniques would miss. The recorded fingerprints are often partially or wholly degraded. For example, these techniques are so sensitive that they record the surface pattern (cloth, wood, paper, skin) on which the fingerprint was found. Also, these latent fingerprints are inherently degraded because of the way they are deposited. They are often smudged or smeared. The result is that the ridge information that identifies a fingerprint is hidden. It can be uncovered and identified using image enhancement techniques. The problem is to remove the degradation while maintaining the integrity of the fingerprint.

2.2 Optical Image Enhancement

An optical processor is typically small and inexpensive. It is fast, but it is not very flexible. It can, however, be a powerful device when it is used for certain applications [17-18].

A conventional coherent optical processor can easily be used to perform three mathematical operations: multiplication, convolution,

and Fourier transformation [19]. These provide the basis for enhancing an image by filtering its Fourier spectrum.

2.2.1 Fourier Transformation

The optical properties of a converging lens are well known [20]. When it is used with a coherent light source, such as a laser, it can perform a two-dimensional Fourier transformation. One possible geometry for obtaining optical Fourier transforms is shown in Figure 2-3. The intensity distribution I(u,v) in the output plane P2 of a converging lens is the squared modulus of the Fourier transformation of the input f(x,y) in plane P1 where the input is illuminated by a coherent plane wave. Mathematically, this is stated as

$$I(u,v) = |F(u,v)|^2 = |\mathcal{F}[f(x,y)]|^2$$

$$= \left| \int_{-\infty}^{\infty}\int f(x,y) \exp[-j2\pi(xu+yv)]\, dx\, dy \right|^2$$

where $u=x_f/\lambda f$ and $v=y_f/\lambda f$

f is the focal length of lens L1,

λ is the wavelength of the coherent source,

and x_f, y_f are distances measured in meters along the u and v axes, respectively, in the Fourier plane P2.

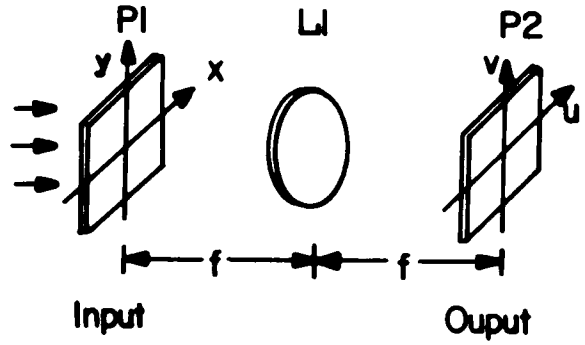

Figure 2-3. Focal Plane-to-Focal Plane Fourier Tranform Geometry.

2.2.2 Spatial Filtering

The superposition integral describes the relationship between the input f(x,y) and the output g(x,y) images of a linear space-invariant system. The integral

$$g(x,y) = \int_{-\infty}^{\infty}\int f(\xi,\eta)h(x-\xi,y-\eta)d\xi d\eta$$

is the convolution operation g(x,y)=f(x,y)*h(x,y) where h(x,y) is the impulse response of the system and * is the convolution operation [21].

In Fourier analysis, convolution in space corresponds to multiplication in spatial frequency. Thus, the Fourier spectra of the input and output spatial distributions are related by G(u,v)= F(u,v)H(u,v) where H(u,v) = $\mathcal{F}$ [h(x,y)] is the coherent transfer function of the processor [22].

A coherent optical processing system is capable of performing linear space-invariant operations. The two-lens geometry shown in Figure 2-4 performs two sequential Fourier transformations and a multiplication operation. Lens L1 collimates the light from the point source, resulting in a coherent plane wave incident on the input image (i.e., a fingerprint) f(x,y) in plane P1. Lens L2 Fourier transforms the input spatial distribution f(x,y). Plane P2 contains a spatial filter H(u,v) that modifies the spectral content of the input spectrum F(u,v). Since F(u,v) is formed in plane P2, this is simply the product relation shown earlier. Lens L3 transforms the output spectrum G(u,v). The output intensity distribution I(x', y') is displayed in plane P3. It is given by $I(x',y') = |g(x',y')|^2$ where g(x',y') is a

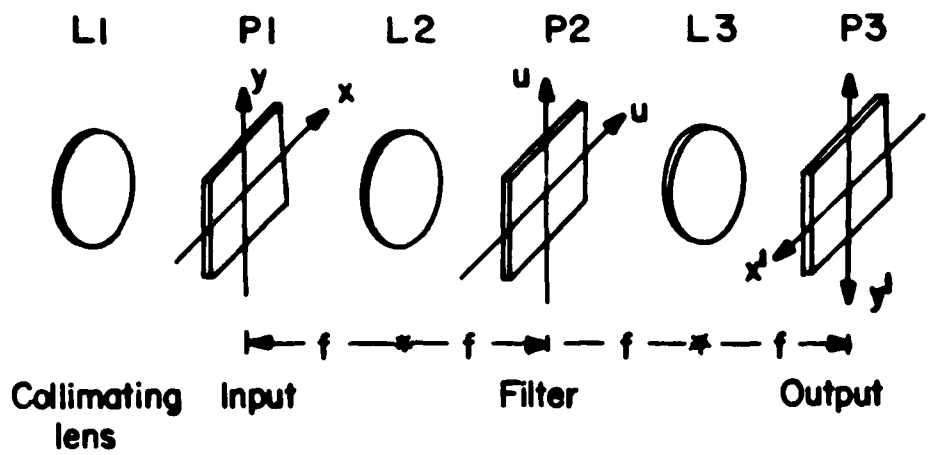

Figure 2-4. A Two Lens Optical Image Processing and Spatial Filtering System.

filtered version of the input image. Note that the coordinates (x', y') of P3 are inverted with respect to (x,y) of P1 because a lens can only perform a forward, and not an inverse, transformation.

A coherent optical processor is able to perform image processing and image enhancement using spatial frequency filters [23-24]. If the spatial frequency filters H(u,v) are chosen appropriately, the degradation in a latent fingerprint can be removed or suppressed, yielding an enhanced fingerprint.

The processor shown in Figure 2-3 is used to locate and analyze the input fingerprint spectra, and the processor in Figure 2-4 is used to enhance input fingerprints. These two processors identify separate areas of this thesis: (1) the identification and location of the important information in the spatial frequency domain (2) the enhancement of that information.

CHAPTER III

LOCATION OF THE RIDGE SPECTRA

If a fingerprint's spectrum is filtered arbitrarily, the identifying features in the fingerprint could be destroyed or altered unknowingly. Therefore, before fingerprints can be enhanced, the spectra of the ridge patterns and the ridge characteristics (minutiae) have to be located within the overall spectrum of the fingerprint. The spectral information that is essential for uniquely identifying a fingerprint will then be known.

In this chapter, the ridge pattern of a fingerprint and the general features in its spectrum are related by comparing the mathematical and experimental results. The spectra of commonly found minutiae were obtained using both a coherent optical processing system and a digital image processing system. The resulting spatial frequency patterns are analyzed and compared to determine the location of the vital information.

Throughout this chapter numbered arrows (1⟶) will be used to point out details in the figures. These details will help clarify descriptions or explanations in the text. The arrows that appear in the text and the figures correspond if they have the same number.

3.1 The Ridge Pattern

The task here is to determine which features in the spatial frequency pattern correspond to the ridge patterns in the input fingerprint. This is done mathematically using Fourier transform pairs as models and by comparing the experimental results obtained using diffraction pattern sampling [25]. The experimental results are presented in a separate section.

3.1.1 Simple Modeling

Simple mathematical models relate the spatial pattern and the spatial frequency pattern of a fingerprint. These models are developed using elementary two-dimensional Fourier transform pairs. These pairs form patterns that approximately describe a fingerprint and its spectrum. As these models are developed, the essential ridge pattern information and its location in the spatial frequency domain will become more apparent. As an example, the tented arch fingerprint and its spectrum, shown in Figures 3-1 and 3-2, respectively, are modeled. This fingerprint and its spectrum will be referred to throughout this thesis.

The most obvious details in Figures 3-1 and 3-2 are the periodicity of the fingerprint ridges and the unique shape of its spectrum. We can model the periodic ridges on the left ($1\longrightarrow$) and right ($2\longrightarrow$) sides of the fingerprint in Figure 3-1 as periodic impulse-sheets (an impulse-sheet is a one-dimensional Dirac delta function described two-dimensionally, i.e., $f(x,y) = \delta(x)$ or

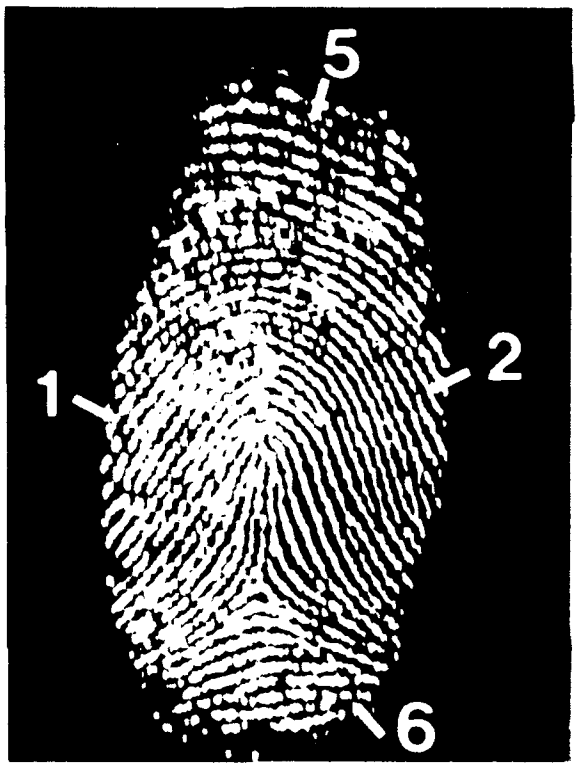

Figure 3-1. A Tented Arch Fingerprint.

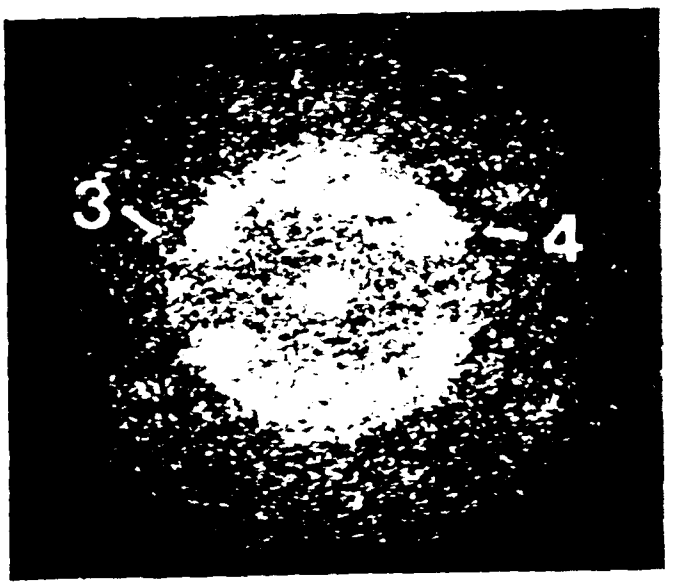

Figure 3-2. The Spectrum (Power Spectrum or Fraunhofer Diffraction Pattern) of the Fingerprint Shown in Figure 3-1.

$f(x,y) = \delta(y)$). The Fourier transformation of uniformly spaced, parallel impulse-sheets is a string of impulses (an impulse is a two-dimensional Dirac delta function, i.e. $f(x,y) = \delta(x,y)$) [26]. The direction of the string of impulses is orthogonal to the direction of the impulse-sheets. Thus, the periodic ridges on the left (1⟶) are mapped by Fourier transformation to a series of impulses (3⟶) in the spatial frequency pattern in Figure 3-2. Using the same Fourier transform pair, the periodic ridges on the right (2⟶) are mapped to a series of impulses (4⟶) in the spectrum. The zero-order impulses for both strings of impulses are located at the center (origin) of the spectral pattern. The zero, first, and second-order impulses are visible in Figure 3-2.

Curved ridges (5⟶) form the transition between the periodic ridges on the left (1⟶) and right (2⟶) sides of the fingerprint. These curved ridges look like periodic arches. They can be modeled as short impulse-sheets that are connected together and change direction so they approximately follow the curve of the arches. With the Fourier transform pair used earlier, the short impulse-sheets are mapped to a series of impulses that are perpendicular to the impulse-sheets. As the approximation to the curve becomes better (the number of links is increased), the series of impulses in the spectrum approaches a continuous arc. Since the angle swept out by the arches is the same as the angle swept out by the arcs, the first-order arcs connect the first-order impulses and the second and succeeding-order arcs connect the second and

succeeding-order impulses. The first and second-order arcs are visible in Figure 3-2.

If the horizontal ridges (6⟶) at the bottom of the fingerprint in Figure 3-1 are modeled as impulse-sheets, then they also map into the integer-ordered arcs in the spectrum (assuming the ridge periodicity is the same). The spectra of the impulse sheets representing the vertical and near-vertical ridges of the fingerprints are distributed horizontally about the origin of the spectral pattern.

The models of the fingerprint and its spectrum that have been described are shown in Figures 3-3 and 3-4, respectively. These models are approximations; they don't completely describe the patterns. First of all, the ridges have been modeled as impulse-sheets. Actually, the distribution of light along a line that intersects the fingerprint ridges orthogonally resembles a biased sinusoid [27]. The spatial frequency pattern in Figure 3-2 agrees. There is less energy in the second and succeeding-order annular rings than in the first-order annular ring. Secondly, the ridges are not uniformly spaced, and they are not exactly alike. This corresponds to the fact that the annular rings have a finite bandwidth.

3.1.2. Diffraction Pattern Sampling

The spectra of fingerprints were analyzed to find the spatial frequency features that correspond to the ridge patterns. Spatial

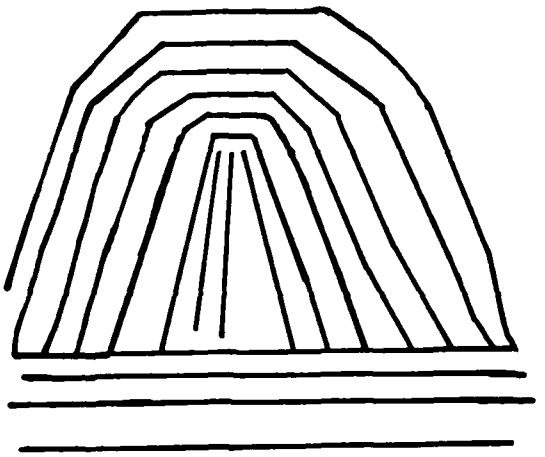

Figure 3-3. A Simple Model of the Tented Arch Fingerprint Shown in Figure 3-1.

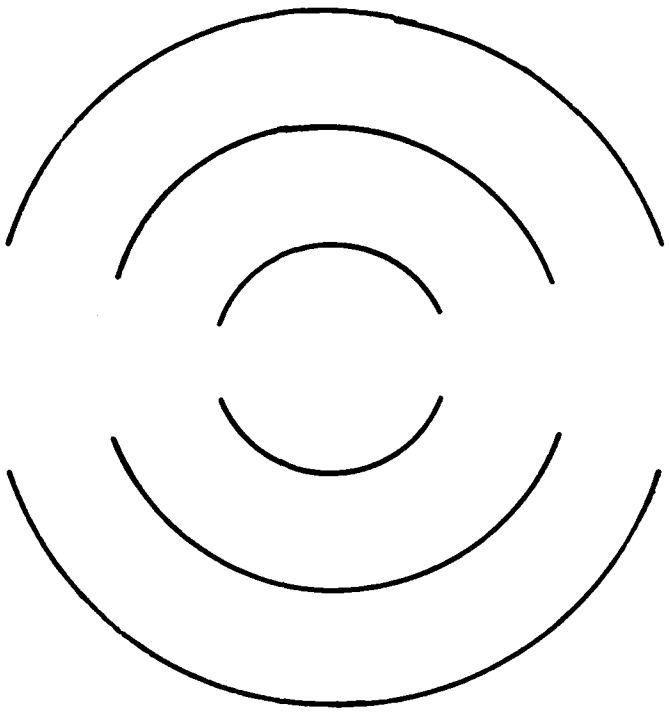

Figure 3-4. A Simple Model of the Power Spectrum Corresponding to the Fingerprint Model in Figure 3-3.

filters were used in a coherent optical processor to sample fingerprint diffraction patterns. These samples were compared with the filtered fingerprints at the output of the processor (the Fourier transform of the spectral sample) to determine which features in the spatial and spatial frequency patterns correspond.

The spatial filters were designed to sample the features of an input fingerprint's spectrum. The two geometrical shapes that were appropriate as sampling filters were a wedge and a circle. An example of a wedge filter is shown in Figure 3-5. It is scale invariant; the same filter can be used for different size input fingerprints. It is a directional filter; it samples (transmits) ridges oriented in a specific direction with respect to the orientation of the filter. The circular filters can be lowpass, bandpass, or highpass filters. They are rotationally invariant, but their size is determined by the type of system and the size and type of input fingerprint. An example of a circular filter is shown in Figure 3-6.

The actual system that was used to locate the vital information in the spatial frequency domain is shown in Figure 3-7. This system was also used to enhance latent and degraded fingerprints, but that is discussed in Chapter IV. Actually, this was a folded system. The direction of light propagation was changed by mirrors M1 and M2, respectively. The mirrors were the boundary between the first and second Fourier transformations.

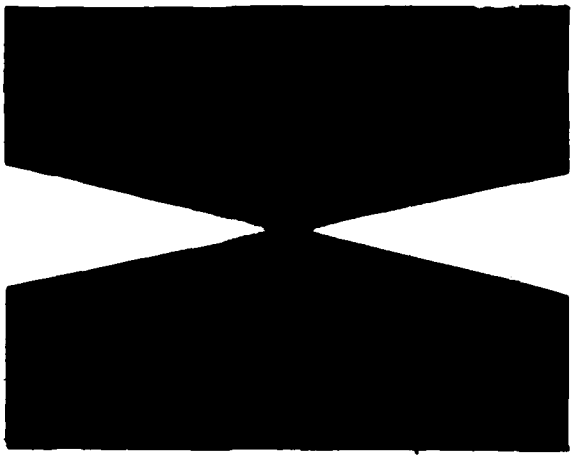

Figure 3-5. A Wedge Filter.

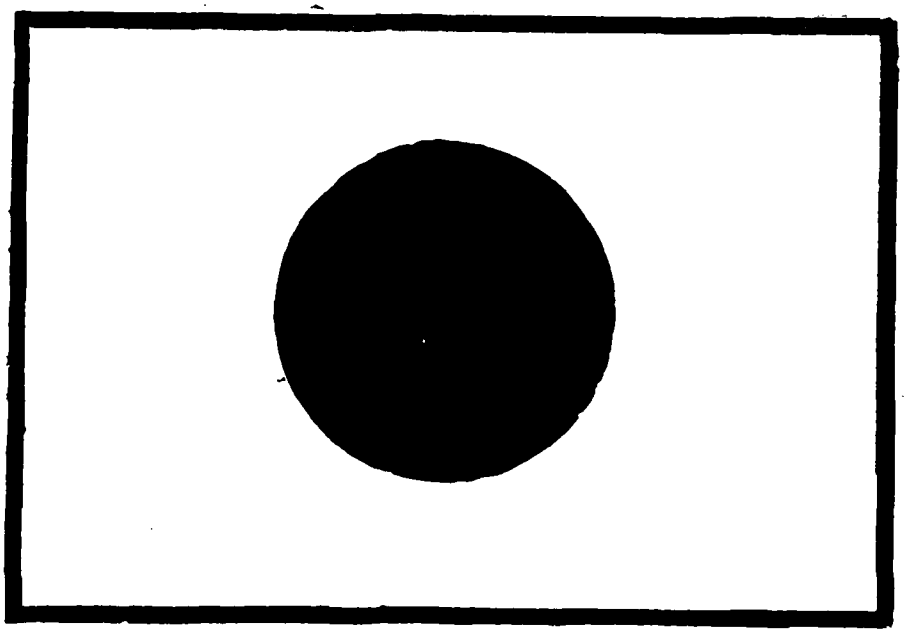

Figure 3-6. A Circular Filter.

Figure 3-7. The Coherent Optical Processing System.

The system had two possible outputs. The first output (7 ⟶) was the diffraction pattern of the input fingerprint. A schematic diagram of this subsystem is shown in Figure 2-3. To view this output, the diffraction pattern (7 ⟶) was magnified by removing mirror M1 and positioning a microscope objective in the Fourier plane (corresponding to plane P2 in Fig. 2-3). The magnified diffraction pattern could then be displayed on a screen behind the microscope objective. This output was used for viewing the spectrum of the input fingerprint and for generating and aligning the spatial filters. The second output was viewed with the system configured as shown in Figure 3-7 (as a coherent optical processing system). A schematic diagram of this system is shown in Figure 2-4. In this configuration, the spectra of the input fingerprints could be filtered for the purpose of isolating the important features. The magnified output of the system (corresponding to plane P3 in Fig. 2-4) was a filtered version of the input fingerprint.

The fingerprints to be analyzed were recorded on film. They were impressed on white paper with black ink, photographically reduced, and input into the system as transparencies. Kodalith film was used because it is a high contrast film. The amount of light in the system was limited by using the positive instead of the negative. This reduced the image degrading interference effects caused by reflections between the system elements.

The spatial filters were also recorded on film. The filters that were used to locate spectral information are real and binary;

the transmittance function of the filters was either 1 or 0. The filters were drawn on white paper with black ink. Then they were photographically reduced to the correct size. The size of the filter matched the size of the diffraction patterns of interest. The size of the diffraction pattern was calculated from the size of the input fingerprint. For example, if x is the average spatial period of the fingerprint in Figure 3-1, then the center frequency of the first-order of its diffraction pattern is given by

$$u = 1/x = x_f/\lambda f$$

where $x_f = \lambda f/x$ is the distance to the first-order arc in the Fourier plane, λ is the wavelength of the incident laser light and f is the focal length of the first lens.

The simple models described in section 3.1.1 were verified using wedge and circular filters. The filters were used to sample the fingerprint diffraction patterns. The corresponding spatial patterns were displayed at the output of the coherent optical processor. Experimental results are presented in the next section.

3.1.3 The Results of Sampling Fingerprint Spectra

The wedge filter shown in Figure 3-5 could be oriented to sample any pie-shaped portion of the input spectrum. As an example, Figure 3-8 shows the tented arch fingerprint filtered with the wedge oriented diagonally (θ ↘, $\theta = 45^o$). The filter

Figure 3-8. A Fingerprint Filtered with the Wedge Filter Oriented Diagonally.

transmitted the first and second-order impulses. Likewise, if the wedge filter was oriented horizontally, the vertical ridges would be transmitted. So the wedge filter transmitted the ridge components that were orthogonal to its orientation.

The experimental results using the directional filtering and the mathematical modeling agreed. However, to completely describe (in a general way) the spectral pattern, two dimensions were required. The wedge filter sampled the spectra in the θ-direction of the polar coordinate system (r,θ). The r-direction was sampled by circular filters.

The circular filters used were ideal highpass and ideal bandpass filters. Since the imaging system that has been used required that the size of the spatial filter change for every change in the size of the input fingerprint, the circular filters were specifically designed for one input fingerprint; the tented arch shown in Figure 3-1. This limitation can be overcome by using an optical processor that can compensate for a change in scale without changing the physical size of the filter [28]. The circular filters used here and the corresponding output images are shown in Figures 3-9 through 3-13. Unless it is stated otherwise, assume that all the binary filters mentioned in this thesis pass the zero frequency component. By passing the zero frequency component, the filtered fingerprint has a constant bias (intensity) level that the imaged fingerprint varies about. Since these intensity variations are less than the DC bias (i.e., the field quantities are not

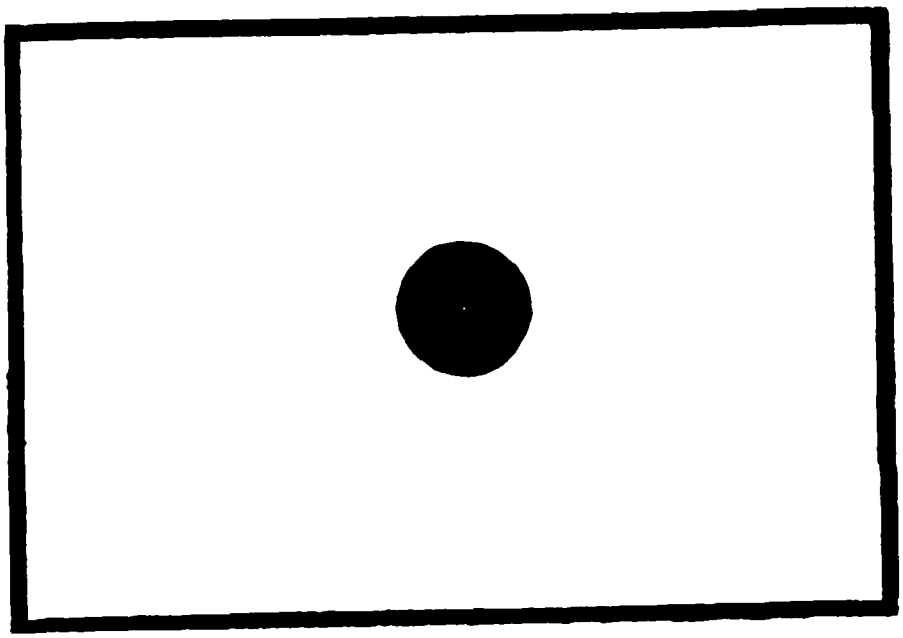

(a)

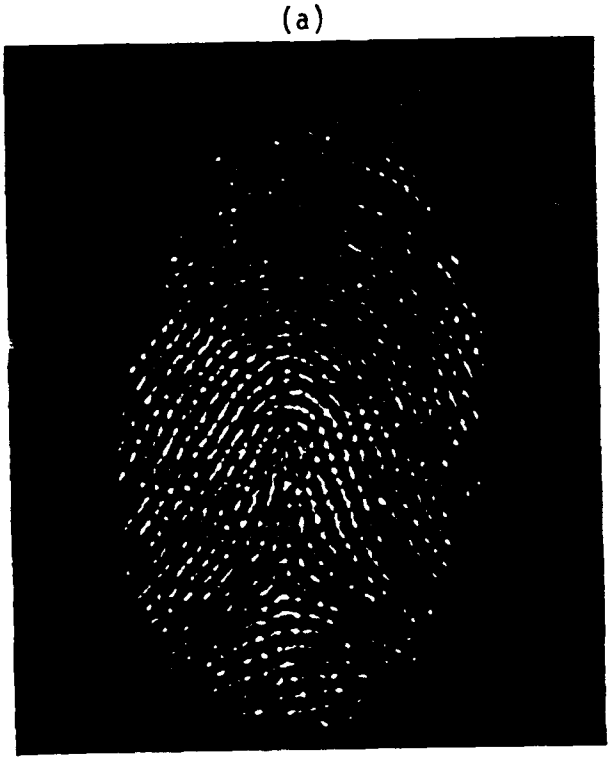

(b)

Figure 3-9. Highpass Filtering Passing Both Frequency Bands. (a) An Ideal Highpass Filter. (b) The Fingerprint After Being Filtered by the Highpass Filter in (a).

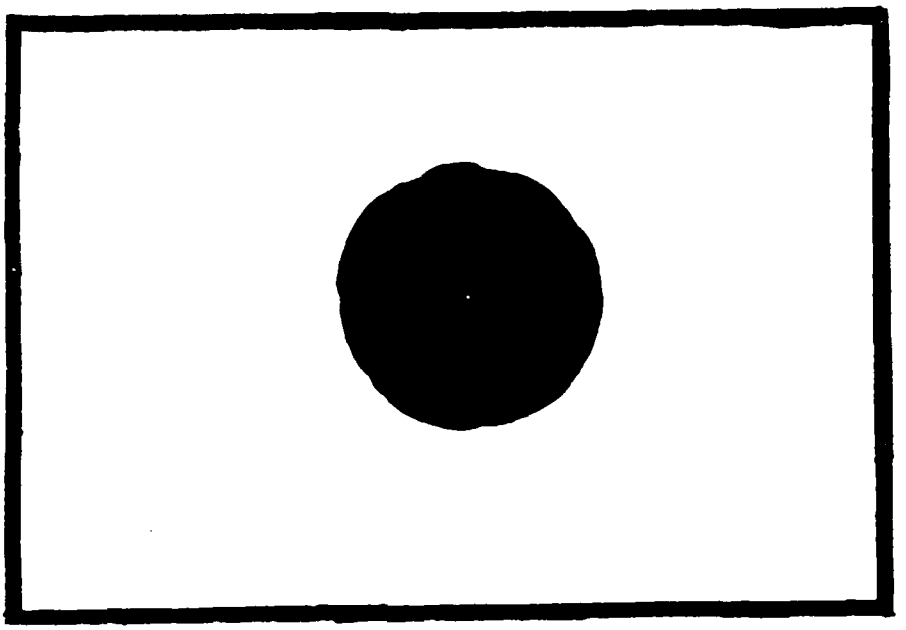

Figure 3-10. Highpass Filtering Passing Second-Order Band. (a) An Ideal Highpass Filter with a Higher Spatial Frequency Cutoff.

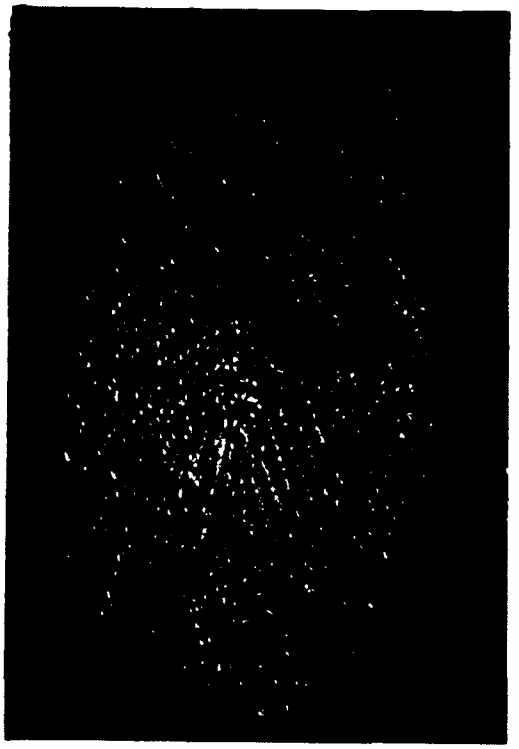

Figure 3-10. (Continued) (b) The Resulting Filtered Fingerprint.

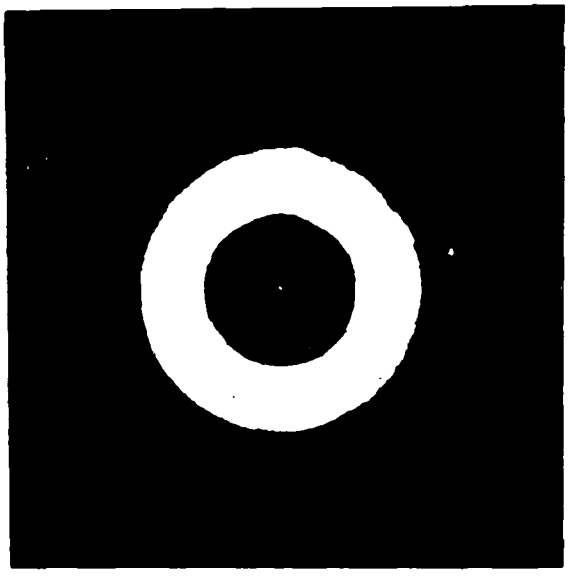

Figure 3-11. Bandpass Filtering Passing First-Order Band. (A) An Ideal Bandpass Filter that Passed Only the First-Order Annular Band of Frequencies (and the Zero Frequency Component).

Figure 3-11. (Continued) (b) The Resulting Filtered Fingerprint.

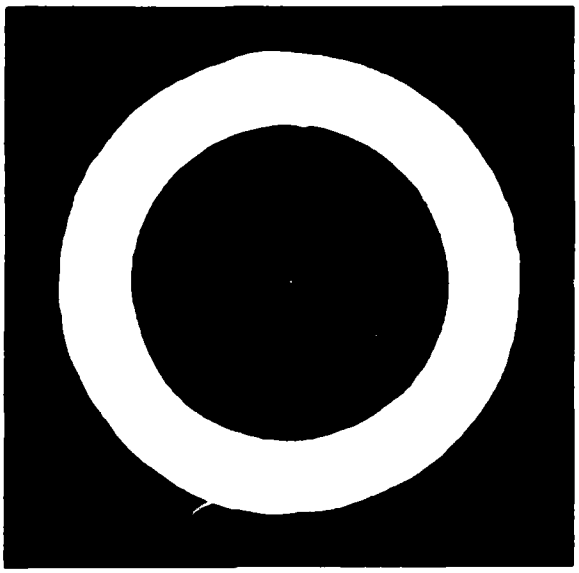

(a)

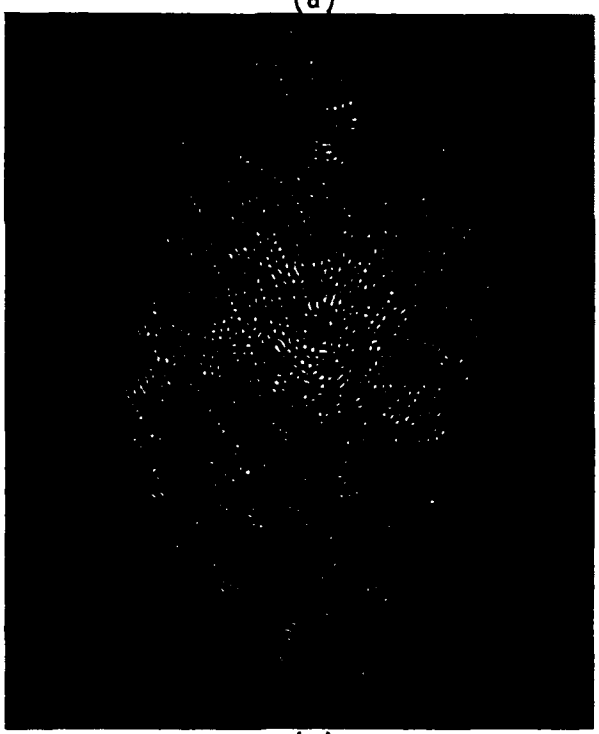

(b)

Figure 3-12. Bandpass Filtering Passing Second-Order Band. (a) An Ideal Bandpass Filter that Passed Only the Second-Order Band of Frequencies (and the DC Term). (b) The Resulting Filtered Fingerprint.

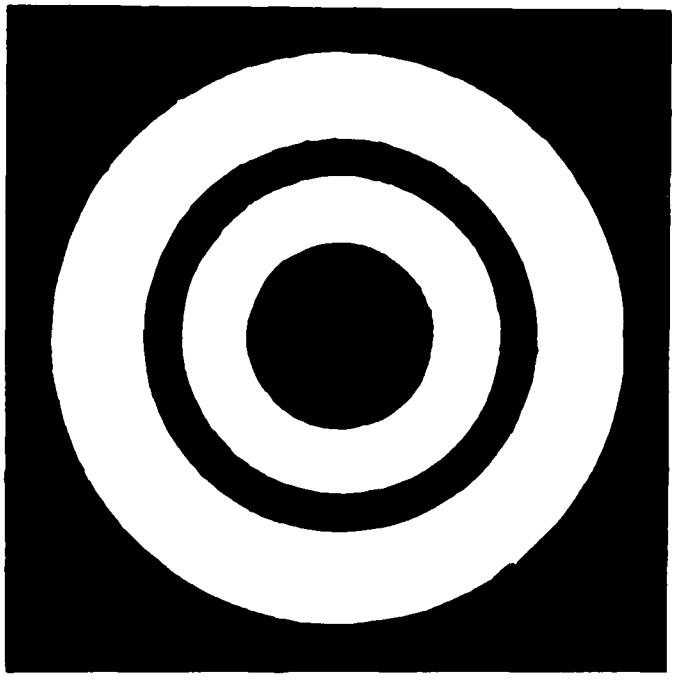

Figure 3-13. Bandpass Filtering Passing First and Second-Order Bands. (a) An Ideal Double-Bandpass Filter that Passed the First and Second-Order Bands of Spatial Frequencies and the DC Term.

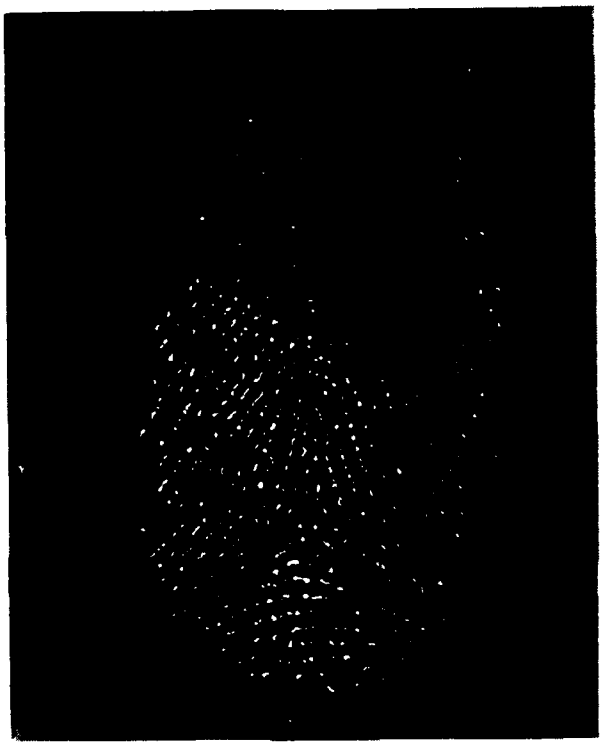

Figure 3-13. (Continued) (b) The Filtered Fingerprint.

negative), the filtered fingerprints displayed have a wider possible range of contrast.

Figures 3-9a and 3-10a are highpass spatial filters. The cut-off frequency for the filter in Figure 3-9a is slightly less than the lowest frequency of the first-order band of spatial frequencies. The corresponding filtered fingerprint, shown in Figure 3-9b, shows that most of the ridge information was transmitted. The highpass filter shown in Figure 3-10a only transmits the spectrum beyond the first-order band of frequencies. Accordingly, Figure 3-10b shows that there is ridge information at these higher frequencies.

Figures 3-11a, 3-12a, and 3-13a are ideal bandpass filters with DC pass. They transmitted the first-order, second-order, and first and second-order bands of spatial frequencies, respectively The resulting fingerprints are shown in Figures 3-11b, 3-12b, and 3-13b. The highpass part of the bandpass filters in Figures 3-11a and 3-12a dominated the lowpass part. Consequently, the ridges were differentiated more than they were integrated (smoothed). Thus, the ridges were edge detected. The multiple peaks shown within each ridge indicate that the ridges (or the image of the ridges) were rough. However, there are still twice as many ridges in the fingerprint in Figure 3-12b as in the fingerprint in Figure 3-11b. If a line is drawn between any two points in each filtered fingerprint, the number of ridges intersecting that line in Figure 3-12b is double that of Figure 3-11b. This shows that the second

band of frequencies is a harmonic of the first band. Figure 3-13b contains most of the ridge information. The highpass filtered fingerprint in Figure 3-9b and the double-bandpass filtered fingerprint in Figure 3-13b are very similar.

From these observations, the following can be concluded: (1) most of the ridge spectra information can be found in the first and second-order bands of spatial frequencies and (2) the integer-ordered bands of spatial frequencies are harmonic frequencies of the first-order (fundamental) band. These conclusions, as shown in Appendix A, are generally true for any type of fingerprint. In the next section, the spectra of the minutiae are located within the overall spectrum of a fingerprint.

3.2 The Minutiae Spectra

The spectra of three types of minutiae (bifurcation, enclosure, and short independent ridge) were located using a coherent optical processing system and a digital computer and image processing system. The minutiae were obtained from the fingerprint in Figure 3-1.

3.2.1. Using a Coherent Optical Processing System

The spectrum of a minutia was obtained by using a small aperture (diameter=1.5 mm) to scan the fingerprint at the input of the processor. The other ridge structure included in the aperture

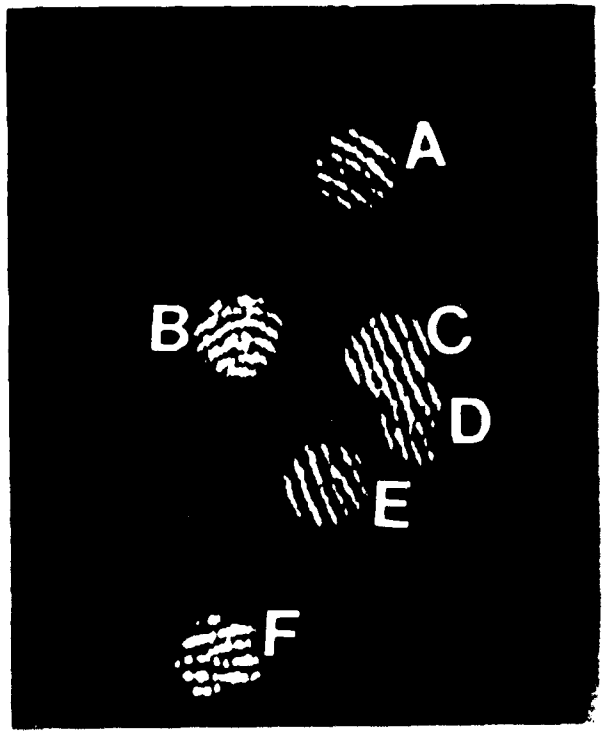

Figure 3-14. Minutiae Isolated Using the Optical Processor. (a) A Short Independent Ridge or Island; (b) An Enclosure or Lake; (c) Periodic Ridges Only; (d) A Bifurcation or Fork; (e) A Bifurcation; (f) A Bifurcation.

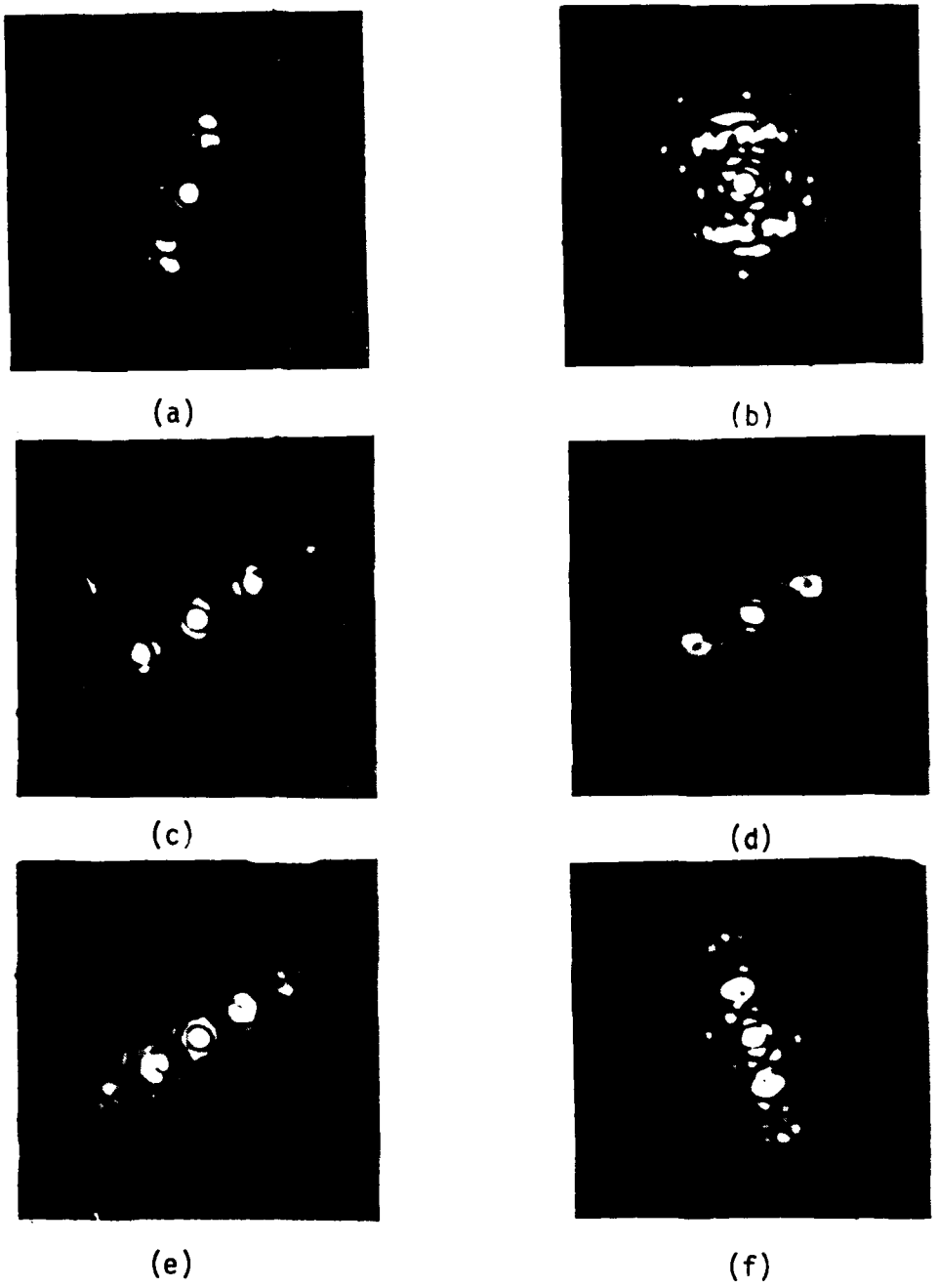

Figure 3-15. Optically Produced Minutiae Spectra. (a) through (f) are the Corresponding Fourier Spectra of the Patterns Shown in Figure 3-14.

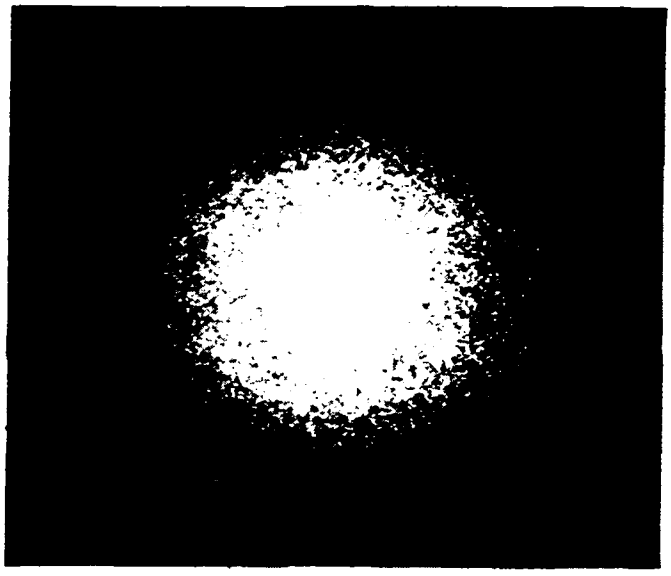

Figure 3-16. The Diffraction Patten of the Tented Arch Fingerprint Shown in Figure 3-1. The Scale was Reduced to Correspond to the Minutiae Spectra Shown in Figure 3-15.

maintained the periodicity of the input. The minutiae are shown and labeled in Figure 3-14 with 3-14(a) being the minutia at the top of the figure and 3-14(f) the minutia at the bottom of the figure. The format of Figure 3-14 was used to show the relative positions of these minutiae within the fingerprint. The diffraction pattern of each of these minutia is shown in Figure 3-15. These minutiae were scaled to the diffraction pattern shown in Figure 3-16.

The spectra of these minutiae can be explained using the Fourier transform pair that was used earlier in this chapter. Fourier transformed periodic ridges map to a series of dots. Figure 3-15b is the exception. The corresponding ridges in Figure 3-14b are not unidirectional. Since these ridges are curved, the intensity of the spectrum is swept out over the same angle as the ridges. If all of the spectra in Figure 3-15 were centered on the diffraction pattern shown in Figure 3-16, they would all be contained within the first, second, and succeeding-ordered annular rings of the overall fingerprint spectrum. All of the spatial frequency patterns have some type of null (blank or black areas in the first and second-order white dots) except the pattern in Figure 3-15c. The corresponding spatial pattern, Figure 3-14c, is the only pattern that does not contain a minutia. In these cases, the nulls in the spectra appear to indicate the presence of minutiae in the spatial pattern.

Just as each minutia is different, each null is also different. The spectrum of the short independent ridge shown in Figure 3-15a has nulls that divide the first-order dots into three parts. The first-order structure of the enclosure's spectrum is divided in half by the null. The first and second-order dots of the spectra in Figure 3-15d, e, and f have a slotted null such that each white dot is shaped like a "C." However, each of these nulls or slots is directed differently with respect to the direction of the string of dots. As expected, though, each one of the bifurcations is also slightly different.

Figure 3-17a is the bifurcation shown in Figure 3-15e without the surrounding ridges included in the aperture (i.e., the input was no longer periodic). Its spectrum was obtained using the Fourier transforming properties of a lens (exactly the same way the other spectra were obtained). Its spectrum is shown in Figure 3-17b. The nulls (8⟶) in the first and second-order dots of the spectrum are present. This further verifies that the presence of nulls in the spatial frequency domain indicates the presence of minutiae in the spatial domain.

From these observations, we can conclude the following: (1) the spatial frequencies of the minutiae are located in the integer-ordered bands of spatial frequencies in the spectrum of the fingerprint, (2) the nulls in the diffraction pattern result from ridges that separate, join, or end, and (3) the direction of each of the nulls depends on the geometrical manner in which the ridges

(a)

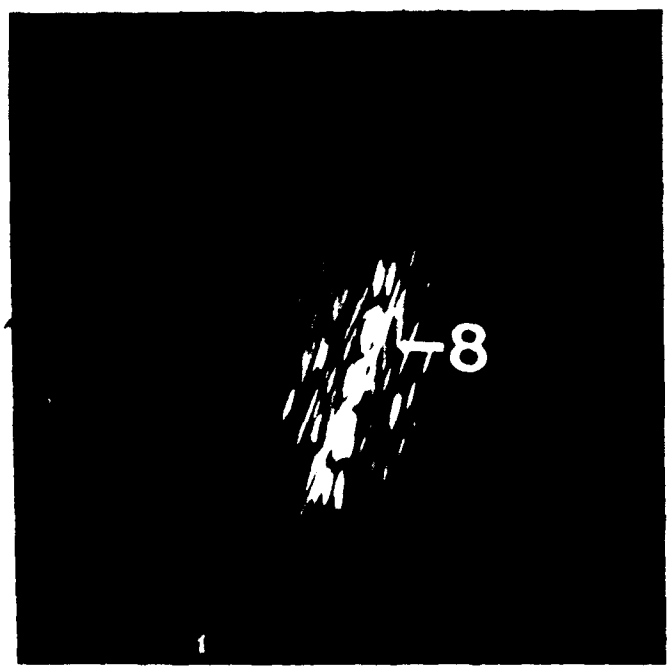

(b)

Figure 3-17. Characteristics of an Isolated Bifurcation. (a) An Isolated Bifurcation Magnified by a Factor of Two. (b) The Spectrum of the Bifurcation Shown in (a).

separate, join, or end. These conclusions will be commented on further in Chapter V.

As the next step, the minutiae were isolated and analyzed using a computer. For this investigation, the fingerprint that has been used in the optical system was digitized and used as the input to the digital system. Thus, continuity was maintained.

3.2.2 Using a Digital Computer and Image Processing System

The VAX 11/780 digital computer and the COMTAL VISION ONE/20 image processing and display system were used to isolate minutiae and to compute and display their power spectra. The same minutiae were isolated within a rectangular aperture as shown in Figure 3-18. The same lettering format as Figure 3-14 was used. The Fast Fourier Transform (FFT) algorithm was performed on these images. Figure 3-19 shows the Fourier transform of these images after they have been enlarged and their histograms have been equalized (or stretched) and shifted to increase the contrast [29]. The spectra that resulted are very similar to spectra obtained using the coherent optical processor. As an example, compare the spectrum in Figure 3-19d (computer processed) with the spectrum of the same minutia shown in Figure 3-15f (optically processed). They are strikingly similar. The cross pattern in each spectrum shown in Figure 3-19 is the intensity distribution of a sinc-squared function. This is an artifact introduced by the aperture since the sinc function is the Fourier transform of a rectangle (i.e., the

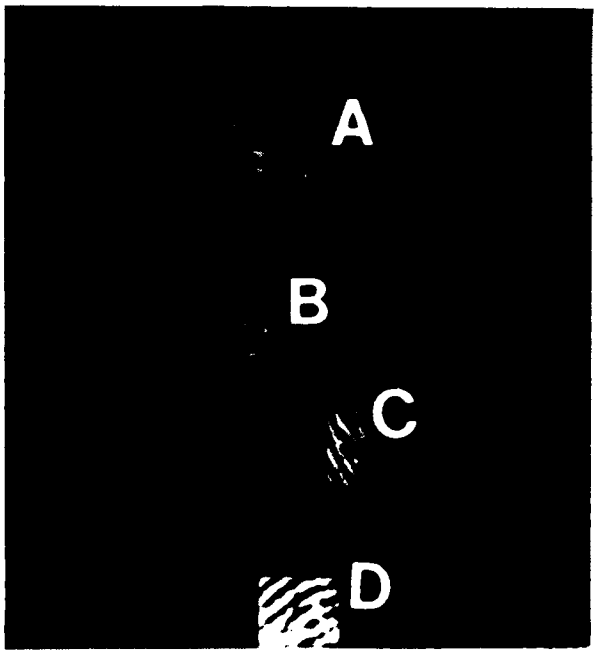

Figure 3-18. Minutiae Isolated Using a Digital Image Processing System. (a) A Short Independent Ridge; (b) An Enclosure; (c) A Bifurcation; (d) A Bifurcation.

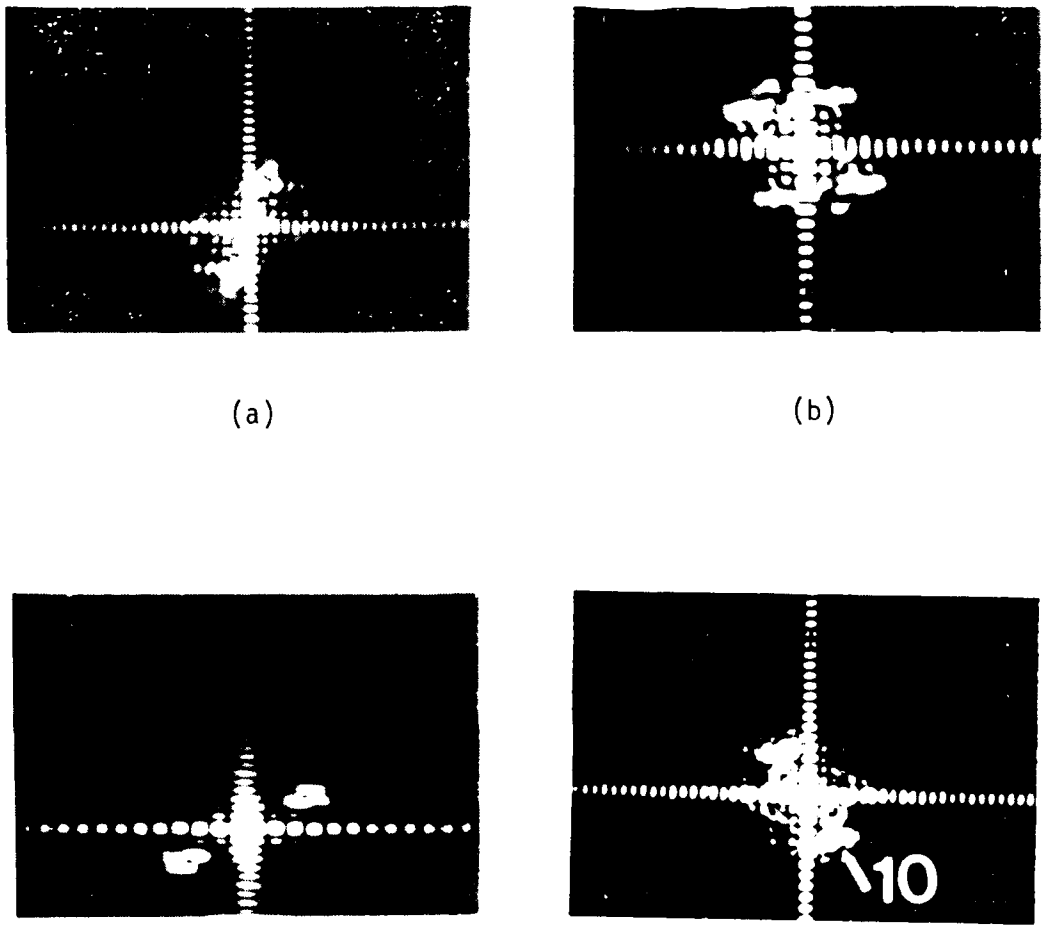

(a) (b)

(c) (d)

Figure 3-19. Digitally Produced Minutiae Spectra. (a) through (d) are the Corresponding Spectra of the Minutiae Shown in Figure 3-18.

rectangular apertures in Figure 3-18). As before, the spectra are located within the integer-ordered bands of spatial frequencies.

The isolated bifurcation that resulted is shown in Figure 3-20a. It was magnified by a factor of two. The corresponding spectrum is shown in Figure 3-20b. It was not magnified. The nulls (9⟶) in this isolated spectrum correspond to the nulls (10⟶) in Figure 3-19d.

Again, the presence of the nulls (9⟶, 10⟶) in the spatial frequency pattern indicates the presence of minutiae in the corresponding spatial pattern and the frequency of these nulls falls within the integer-order bands of spatial frequencies in the spectrum of the fingerprint.

3.3 Discussion

The experimental results show that the spectra of the ridges and the minutiae are located in the integer-ordered (harmonic) spatial frequency bands in the fingerprint's diffraction pattern. We also discovered that the nulls in these spatial frequency bands result from the minutiae in the spatial domain. The distance from the center of the diffraction pattern and the angular position of the null correspond to the spatial frequency and angular orientation position of the minutiae in the fingerprint (position in space translates to phase information in spatial frequency which cannot be detected using intensity recorders). This was shown using an optical image processor and a digital image processor. As men-

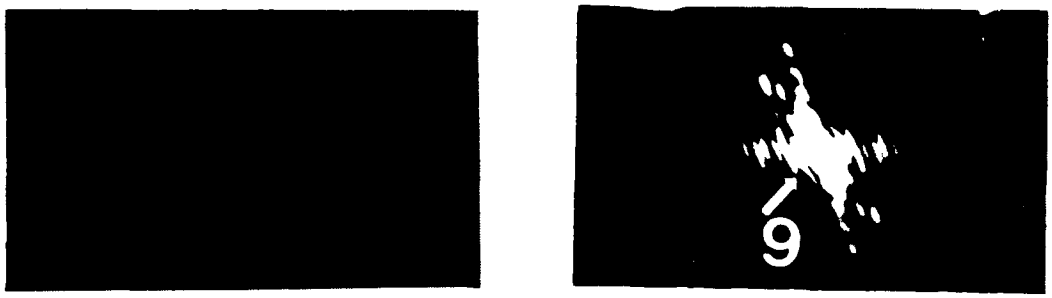

(a) (b)

Figure 3-20. Digitally Produced Bifurcation Characteristics. (a) An Isolated Bifurcation that Corresponds to the Fork in Figure 3-18d. It is Shown Magnified by a Factor of 2. (b) The Spectrum of the Isolated Fork Shown in Figure 3-20a.

tioned earlier, Appendix A shows that these statements are generally true for a wide variety of fingerprint types.

Since the spectra of the identifying fingerprint characteristics have been found to lie in well-defined regions, latent and/or degraded fingerprints can be enhanced without jeopardizing their uniqueness. General binary filters can be used to block spatial frequencies outside the information bearing annular rings without destroying or altering the identifying features of the fingerprints. Thus, these simple, general filters can enhance many types of fingerprints (that is, the shapes of the diffraction patterns are similar for all types of fingerprints).

CHAPTER IV

ENHANCING FINGERPRINTS

Schlieren, Laplacian, and contrast reversal filters and the circular filters (lowpass, bandpass, and high pass) described in Chapter III were used to enhance degraded fingerprints. They form a general set of simple filters that can enhance various types of degraded fingerprints (whorl, central pocket loop, tented arch, twinned loop) by removing or reducing the degradation (smears, smudges, background noise, additive and multiplicative noise).

The Schlieren, Laplacian, and contrast reversal filters are introduced by showing the resulting enhancements of "good" latent fingerprints. Each type of filter and its effect on fingerprints is illustrated and described. Then one or more of the five filters from the general set is used to enhance degraded fingerprints.

4.1 Enhancement Filters

Contrast reversal, Schlieren, and Laplacian filters can be used to enhance any type of fingerprint. They do not depend on the size and shape of the input frequency spectrum (unlike the circular filters discussed earlier). The contrast reversal or zero spatial frequency filter is the limiting case of a highpass filter. It is an ideal highpass filter with an infinitesimal radius (cutoff frequency). It changes the level of contrast in the input fingerprint by altering the zero frequency term. The Schlieren filter is

a directional filter. It is an abrupt, radially-directed, symmetric filter. It performs an edge enhancement by blocking all the spectral components to one side of the zeroth order component. The Laplacian filter is a computer-generated hologram (CGH). It is circularly symmetric. It differentiates the input fingerprint by attenuating the input spectrum as a function of radial distance from the origin.

A contrast reversal filter is a simple zero spatial frequency (DC) blocking filter. The filter is placed in the spatial frequency plane of the coherent optical processor shown in Figure 3-7 and aligned to remove or reduce the zero frequency component of the input fingerprint spectrum. Ideally, the contrast of the input fingerprint can be reversed; the dark valleys become light and the light ridges become dark. In reality, the contrast will be changed, but not reversed unless the ridge-valley duty cycle is different from 50% and the bright area predominates. Figure 4-1(a) shows an unfiltered twinned loop fingerprint recorded at the output of the processor. Figure 4-1(b) shows the same twinned loop with a zero frequency filter applied. The contrast has been changed. The reduction in the zero and low spatial frequency component has reduced the width of the ridges (i.e., the ridges have been thinned and the valleys have been widened) making the ridges slightly more easy to trace. The amount of change in the contrast is determined by the identifiability and readability of the ridges and valleys and depends upon the size and the transmittance of the filter.

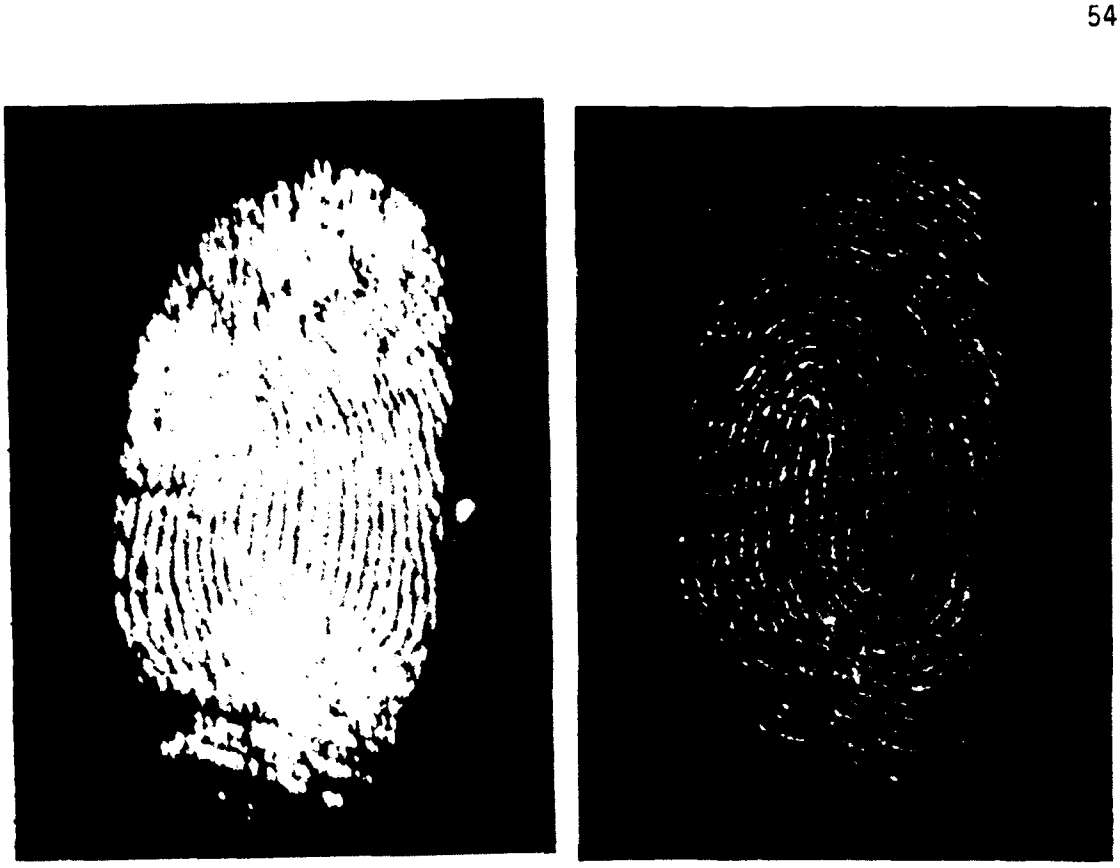

(a) (b)

Figure 4-1. Contrast Enhancement. (a) An Unfiltered Twinned Loop Fingerprint. (b) A Twinned Loop Fingerprint After Being Filtered with a Zero Spatial Frequency Blocking Filter.

Contrast reversal may be useful if the valleys are more readable and identifiable than the ridges.

A Schlieren filter performs a directional edge enhancement. A razor blade or a knife makes a good Schlieren filter. It is positioned to intersect the zero spatial frequency point of the input spectrum and oriented in any direction. The filter enhances the spatial frequency components orthogonal to the knifes edge. Figure 4-2 shows an unfiltered central pocket loop. Figure 4-3 shows a central pocket loop that has been enhanced by a Schlieren filter oriented with its edge along the horizontal frequency axis. The horizontal components of the ridges have been sharpened or edge enhanced. The ridges are easier to trace and the minutiae are more discernable.

A Laplacian filter performs a two-dimensional linear differentiation operation on the input fingerprint. The operation is given by

$$\nabla^2 f(x,y) = \frac{\partial^2 f(x,y)}{\partial x^2} + \frac{\partial^2 f(x,y)}{\partial y^2}$$

where $f(x,y)$ is the two-dimensional input fingerprint. The filter is a computer-generated hologram made according to the Burckhardt CGH method [30-32]. The CGH program was executed on an Apple II computer and the output was plotted on a Radio Shack plotter. The CGH was photoreduced to the appropriate size, placed in the

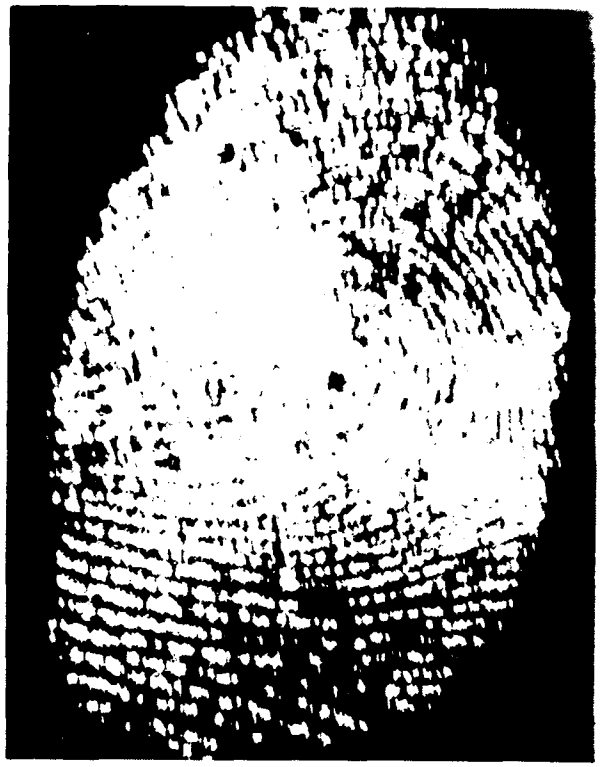

Figure 4-2. An Unfiltered Central Pocket Loop.

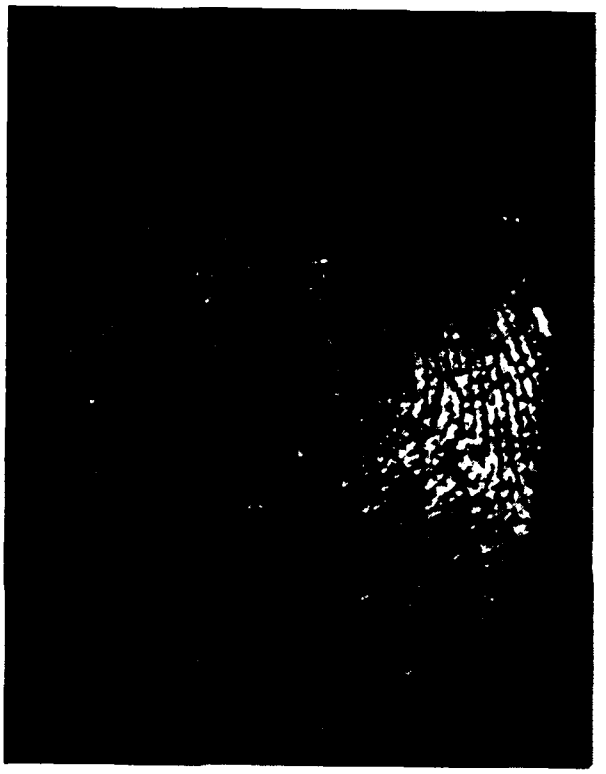

Figure 4-3. A Central Pocket Loop Filtered with a Schlieren Filter.

frequency plane of the processor, and centered on the input spectrum. The CGH samples the input spectrum with a complex array of elements defined by the given function. For the Laplacian CGH, the size (magnitude) of the samples is governed by their radial distance from the center of the hologram. This function is given by

$$r = \sqrt{A(x^2 + y^2)}$$

where r is the distance of the sample from the origin of the filter and A controls the rate which the sample size varies. Figure 4-4 shows a central pocket loop that has been edge enhanced using the Laplacian CGH filter shown in Figure 4-5. Notice by comparing Figures 4-2 and 4-4 that the Laplacian filter removes or reduces the slowly varying changes in intensity. Thus, the distinction between the ridges and the valleys is greater than the distinction in Figure 4-2 and the minutiae are more obvious.

These filters enhanced various types of "good" latent fingerprints. They also can enhance degraded fingerprints. In the next section the general filters were applied to latent fingerprints that have been degraded.

4.2 Enhancing Degraded Fingerprints with General Filters.

In this section, four fingerprints, each with different degradations, were enhanced with one or more filters from the general

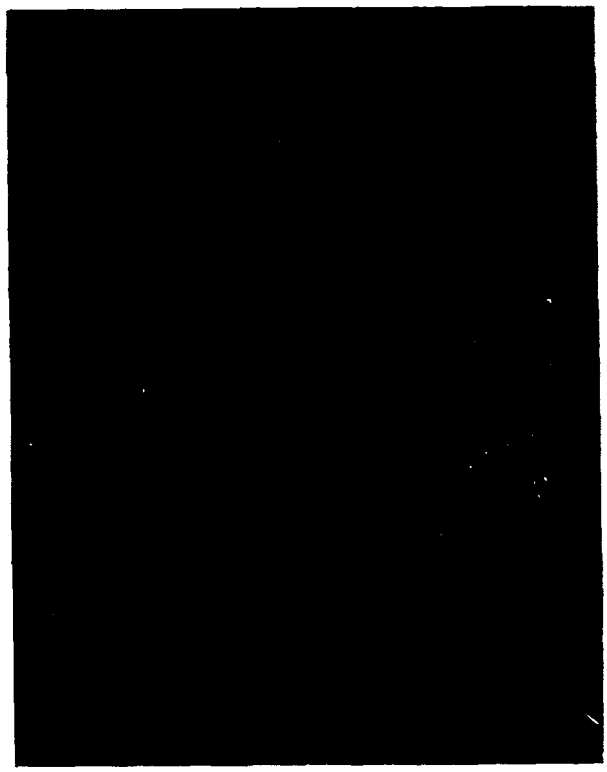

Figure 4-4. A Central Pocket Loop (see Figure 4-2) Enhanced by the Laplacian CGH Shown in Figure 4-5.

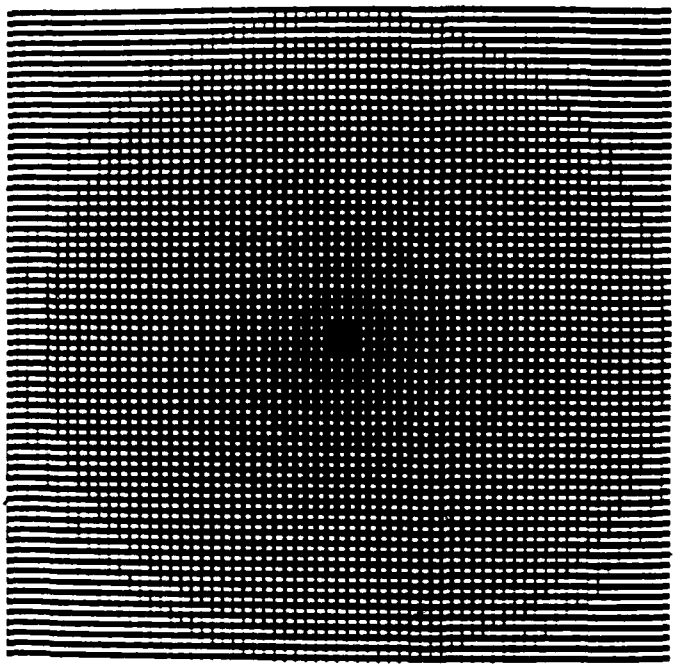

Figure 4-5. A Laplacian Computer-Generated Hologram (CGH) Filter.

set (lowpass, bandpass, highpass, contrast reversal, Schlieren, and Laplacian). An integrator CGH filter was also used. These filters were used in the coherent optical processing system shown in Figure 3-7. The degraded fingerprints were generated by introducing the degradations on "good" latent fingerprints (such as those shown in section 1). Both the degraded fingerprint and its enhancement are shown and discussed.

The first degraded fingerprint, shown in Figure 4-6(a), is a whorl that has been photographed out-of-focus. The ridges and the valleys are fuzzy and lack definition. This degraded fingerprint was partially enhanced using a Schlieren filter. The enhancement is shown in Figure 4-6(b). The edge of the filter was oriented horizontally so the vertical components of the spectrum were enhanced. The ridges upper most in Figure 4-6(b) are clearer and more distinct. The Schlieren filter can be oriented in other directions to enhance the desired spectral components.

Another whorl has been degraded by pressing a finger down on a surface and recording the "flattened" fingerprint. The degraded fingerprint is shown in Figure 4-7(a). There is a lack of contrast between the ridges and the valleys especially in the center of the fingerprint. Figure 4-7(b) shows the enhancement of the degraded fingerprint using a knifes' point Schlieren filter (i.e., like half of a wedge filter). The ridges were enhanced in two directions. There is slight improvement in the readability of the ridges in the center of the fingerprint. A contrast reversal filter did not

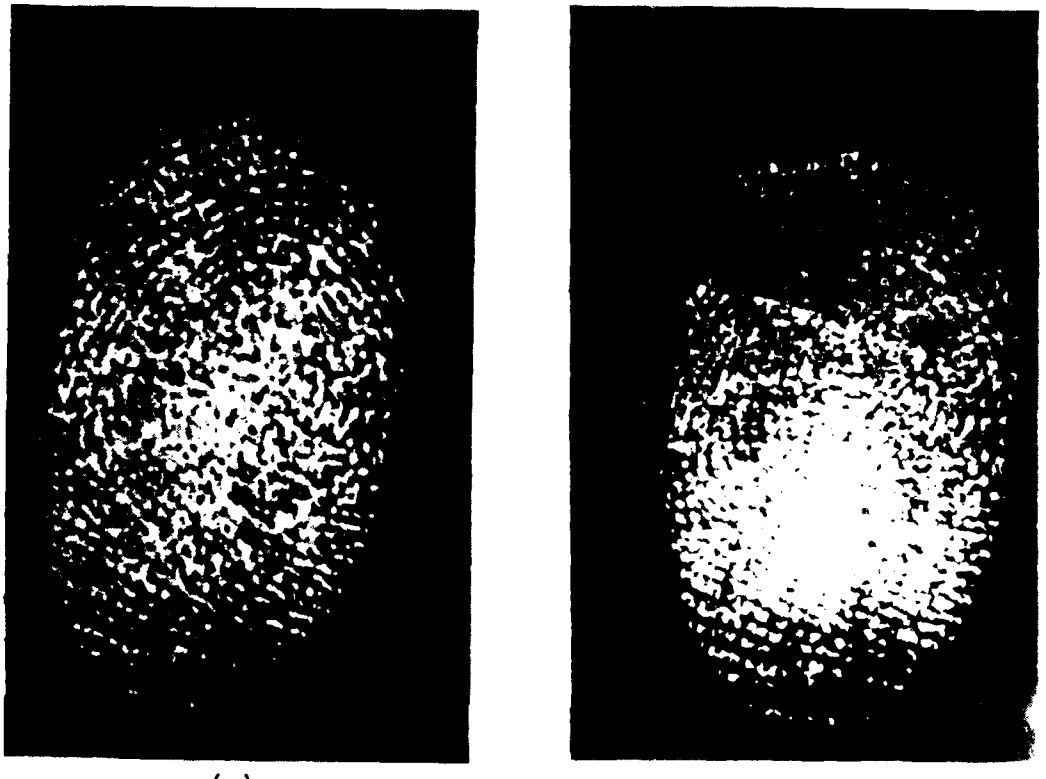

(a) (b)

Figure 4-6. Schlieren Filter Enhancement. (a) An Out-of-Focus Whorl. (b) An Enhancement of Figure 4-6a Using a Schlieren Filter.

(a) (b)

Figure 4-7. Wedge Schlieren Filter Enhancement. (a) A Degraded Whorl. (b) An Enhancement of the Degraded Whorl Shown in Figure 4-7a.

enhance this degraded fingerprint as well because of the lack of difference in intensity between the dark ridges and the slightly darker valleys.

The tented arch shown in Figure 4-8 was degraded by its noisy background. The cross-hatch pattern in the figure is the cloth texture of duct tape. The latent fingerprints left on the duct tape were detected, lifted, and recorded using techniques that use the inherent flourescence of fingerprint residues under laser illumination [33]. The fingerprint and its noisy background were separated using an optical image processor and the appropriate spatial frequency filters.

The degraded fingerprint shown in Figure 4-8 was enhanced using the highpass filter shown in Figure 4-9. Since the spatial frequencies of the background pattern are lower than the first-order spatial frequencies of the fingerprint, the power of the degradation was reduced by using an ideal highpass filter with the cut-off frequency that was slightly less than the lowest frequency in the first-order band of spatial frequencies. The enhanced fingerprint is shown in Figure 4-10. The ridges appear to be a series of disconnected dots. Actually, the dots are the intersections of ribs of the fabric in the duct tape and the ridges of the fingerprint. The effect was reduced by using an integrator CGH filter, shown in Figure 4-11, in combination with a high pass filter. Optically, an integrator CGH is an inverted Laplacian CGH (for a normalized integrator $r = \sqrt{A/(x^2+y^2)}$). This enhancement

Figure 4-8. A Tented Arch Degraded by the Background Texture of Cloth.

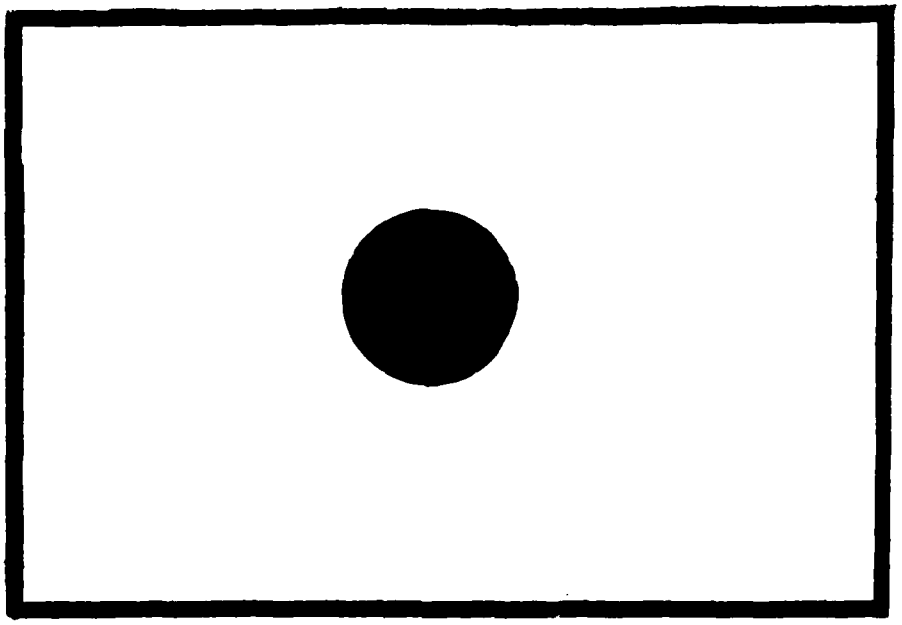

Figure 4-9. An Ideal Highpass Filter.

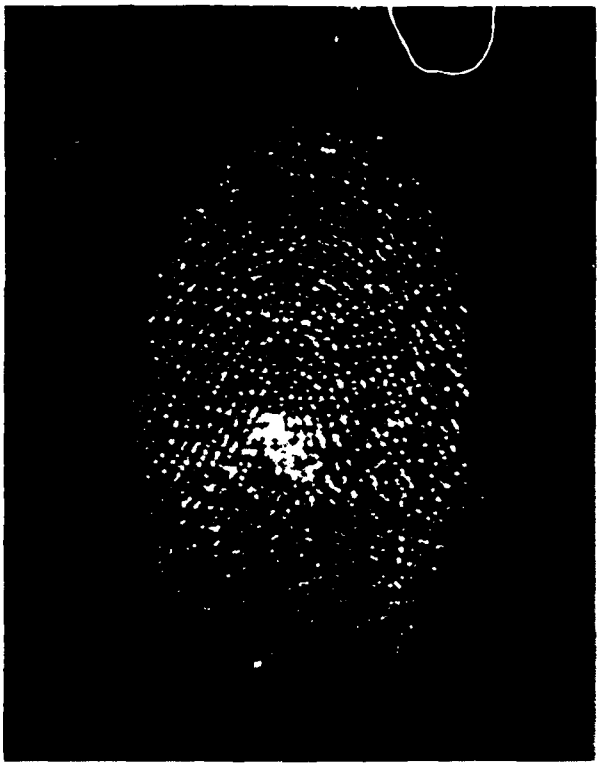

Figure 4-10. An Enhanced Version of the Degraded Fingerprint Shown in Figure 4-8 Using the Highpass Filter Shown in Figure 4-9.

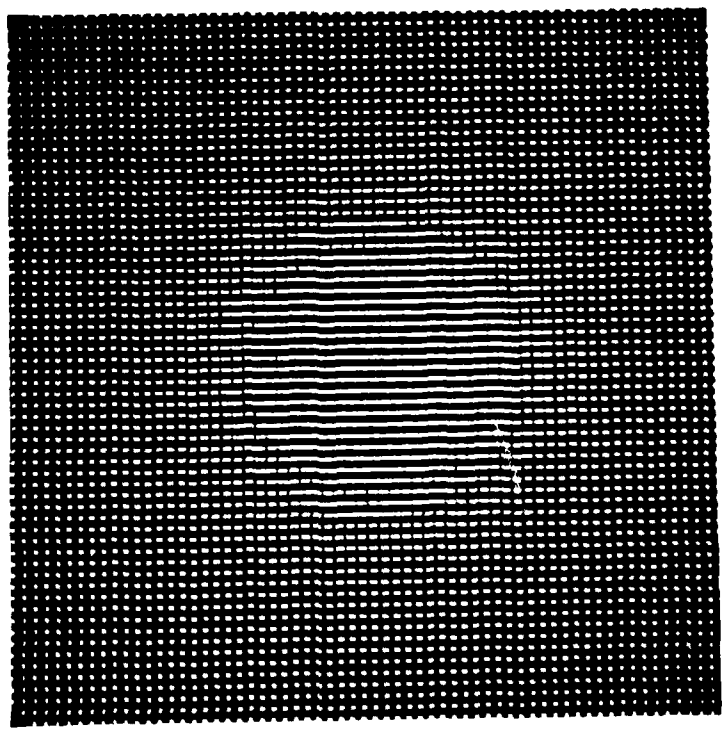

Figure 4-11. An Integrator CGH Filter.

is shown in Figure 4-12. The fingerprint has reduced background noise and clearer and more continuous ridges.

In the final example, a tented arch fingerprint was multiplied by a Gaussian smudge. The degradation was generated on a VAX 11/780 computer and displayed on a COMTAL VISION ONE/20 digital image processing system. The degraded fingerprint, shown in Figure 4-13(a), was photographed from the screen of the monitor (there is a vertical elongation because the camera's aspect ratio differs from the monitor's aspect ratio). The ridges in the central portion of the degraded fingerprint can not be seen. Our eyes can not distinguish the differences in gray levels between the bright ridges and the bright degradation. Figure 4-13(b) shows the degraded fingerprint after a Laplacian filter has been applied. It increased the differences in intensity levels between the slowly varying degradation and the more rapidly changing ridges by differentiating the input degraded fingerprint. The ridges are visible and can be traced. The minutiae can be located. The degraded fingerprint was also enhanced using a highpass filter. The enhancement is shown in Figure 4-13(c). Most of the effect of the low frequency multiplicative degradation has been blocked by the highpass filter. The integrity of the underlying fingerprint has been maintained through the enhancement and the identifying features are more obvious.

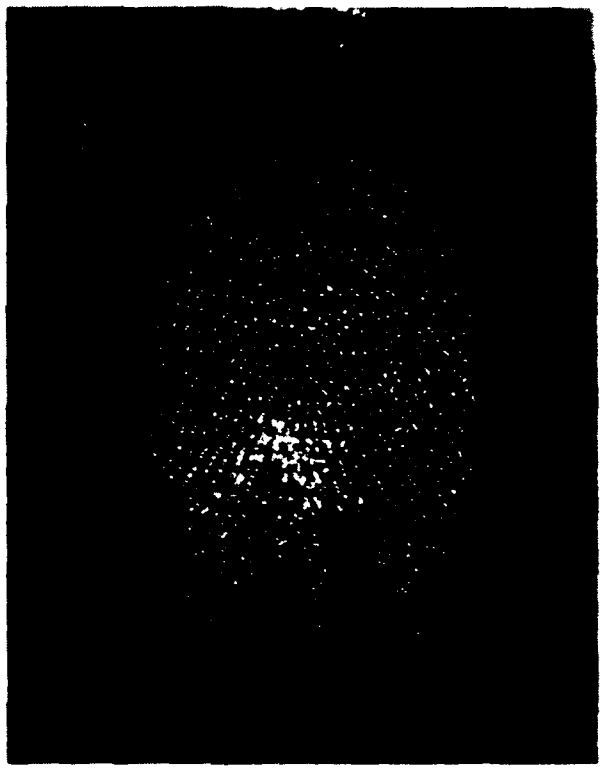

Figure 4-12. An Enhanced Tented Arch Fingerprint Using a Highpass Filter and an Integrator CGH Filter.

Figure 4-13. Enhancement of a Multiplicative Degradation. (a) A Tented Arch Fingerprint Degraded by a Multiplicative Gaussian Smudge.

Figure 4-13. (Continued) (b) An Enhancement of the Degraded Fingerprint in Figure 4-13a Using a Laplacian Filter.

Figure 4-13. (Continued) (c) An Enhanced Tented Arch Fingerprint Using A High-pass Filter.

CHAPTER V

CONCLUSIONS

Optical image processing techniques were used to investigate the spectra of fingerprints and to demonstrate the use of optical filters to enhance degraded fingerprints. A conventional two-lens coherent optical processor was used as the basic system because it was easy to use and theoretically and intuitively simple to understand. Spatial filters were generated and used in the processor to examine the spectra of various types of "good" fingerprints. Specifically, the similarities and differences in the shape and spectral content of the fingerprint spectra were compared and analyzed. It was found that the structure of the spectra were basically the same; the fingerprint ridges were located in harmonic bands of spatial frequencies. It was also discovered that the spectra of the identifying ridges and minutiae, unique to a particular fingerprint, are located within the frequency bands.

To enhance the identifying features of each type of fingerprint, a library of general spatial filters was developed. In keeping with the optical system and the image processing techniques, the optical filters were kept simple. Circular, binary filters were very effective. They enhanced degraded fingerprints by blocking the unwanted and unnecessary spectral components (of the Fourier transformed degraded fingerprints) outside the information-bearing bands of frequencies. By simply removing the

low frequency fuzziness (i.e., smudges and smeared ridges) and the high frequency graininess, the identifiability of latent fingerprints was improved. Removal of the zero frequency term displayed a version of the fingerprint that was potentially easier to identify. Removing part of the spectrum enhanced part of the degraded fingerprint (i.e., specifically directed components). The degraded fingerprints were also differentiated and integrated thus performing an edge enhancement operation or a smoothing operation, respectively, on the degraded fingerprint ridges. Overall, it was demonstrated using simple filters, singly or in combination, that different types of fingerprints could be enhanced without affecting the fundamental ridge structure of the fingerprints. The enhanced fingerprints shown in Chapter IV demonstrated the power of optical image processing used in a well-defined task.

The success of enhancing degraded fingerprints using coherent optical processing techniques warrants extended and expanded investigation. The use of other complex filters and processor geometries has not been studied. Some simple improvements to the existing binary filters such as using apodized apertures and non-ideal filters (i.e., Butterworth and Chebyshev) would reduce the ringing at the output of the processor without sacrificing system simplicity. Other types of complex (i.e., computer-generated holograms) filters would increase the size and flexibility of the filter library. The Hilbert transform is an example. Finally, this research was limited to coherent optical processing

techniques, but incoherent optical processing could be used. It would eliminate the speckle noise and reduce the tight filter positioning constraints required by coherent processing. Although digital processing techniques are more flexible, the simplicity of enhancing degraded fingerprints with a dedicated optical "black box" is very appealing.

REFERENCES

[1] Robert D. Olsen, Sr., Scott's Fingerprint Mechanics, Charles C. Thomas, Publisher, Springfield, IL, (1978).

[2] P. S. Considine and R. A. Gonsalves, "Optical Image Enhancement and Image Restoration," Topics in Applied Physics: Optical Data Processing, 23, D. Casasent: Editor, Springer-Verlag, Berlin Heidelberg (1978).

[3] Harry C. Andrews, "Monochrome Digital Image Enhancement," Applied Optics, 25, 495-503, 1976.

[4] A. F. Lehar, R. J. Stevens, "Image Processing System for Enhancement and Deblurring of Photographs," Optical Engineering, 23, 303-308, 1984.

[5] Adonis E. Barsallo, "Digital Enhancement of Degraded Fingerprints," M.S. Thesis, Texas Tech University, (1985).

[6] Marce Eleccion, "Automatic Fingerprint Identification," IEEE Spectrum, 10, 36-45, 1973.

[7] Donald H. McMahon, Gilbert L. Johnson, Stanley L. Teeter, and Colin G. Whitney, "A Hybrid Optical Computer Processing Technique for Fingerprint Identification," IEEE Transactions on Computers, C-24, 358-369, 1975.

[8] Eleccion, p. 40.

[9] Lindsey McWilliams, "Computer Fingers Criminals," Popular Computing, 29-32, July 1985.

[10] Joseph W. Goodman, "Operations Achievable with Coherent Optical Information Processing Systems," Proc. IEEE, 65, 29-38 1977.

[11] Henry Stark, Applications of Optical Fourier Transforms, Academic Press, Inc., New York, 1982)

[12] Andrews. pp. 501-503.

[13] Royal Canadian Mounted Police, Fingerprints: A National Police Service, Chapters 1-4, 1954.

[14] Olsen, pp. 9-11.

[15] E. Roland Menzel, Fingerprint Detection with Lasers, Marcel Dekker, New York, 1980.

[16] Olsen, pp. 343-353.

[17] Goodman, pp. 29-38.

[18] Stark, pp. 131-205.

[19] Goodman, pp. 29-38.

[20] Joseph W. Goodman, Introduction To Fourier Optics, McGraw-Hill, New York, 1968.

[21] Goodman, pp. 17-20.

[22] Goodman, pp. 110-113.

[23] George W. Stroke, Maurice Haligua, Fredrich Thon, and Dieter H. Willasch, "Image Improvement and Three-Dimensional Reconstruction Using Holographic Image Processing," Proc. IEEE, 65, 39-62, 1977.

[24] Considine, pp. 53-79.

[25] George G. Lendaris and Gordon L. Stanley, "Diffraction Pattern Sampling for Automatic Pattern Recognition," Proc. IEEE, 198-208 (1970).

[26] Lendaris, pp. 200-202.

[27] Barsallo, pp 69-81.

[28] S. H. Lee, "Coherent Optical Processing," Topics in Applied Physics: Optical Information Processing, 48, S. H. Lee: Editor, Springer-Verlag, Berlin Heidelberg, 60-65, 1981.

[29] Barsallo, pp. 39-42.

[30] Scott B. Chase, "Fabrication of Binary Phaser Diffusers for Space-Variant Processing," M. S. Thesis, Texas Tech University, 41-49, 1983.

[31] C. A. Irby, "Computer Generated Multiplex Holography," M. S. Thesis, Texas Tech University, 27-33, 1980.

[32] C. B. Burckhardt, "A Simplification of Lee's Method of Generating Holograms by Computer," Appl. Opt., 9, 1949 1970.

[33] Menzel, pp. 45-77.

APPENDIX

The spectral patterns of many types of fingerprints are quite similar. Five different fingerprints and their spectra are shown in the following figures.

The spectral pattern of these different types of fingerprints are circularly shaped and basically the same size, (even though the fingerprints were obtained from different people). The identifying information is located in harmonic or integer-ordered bands of spatial frequencies. From these similarities, general filters can be developed to enhance, not just a single fingerprint or a single type of fingerprint, but a wide class of fingerprints.

(a)

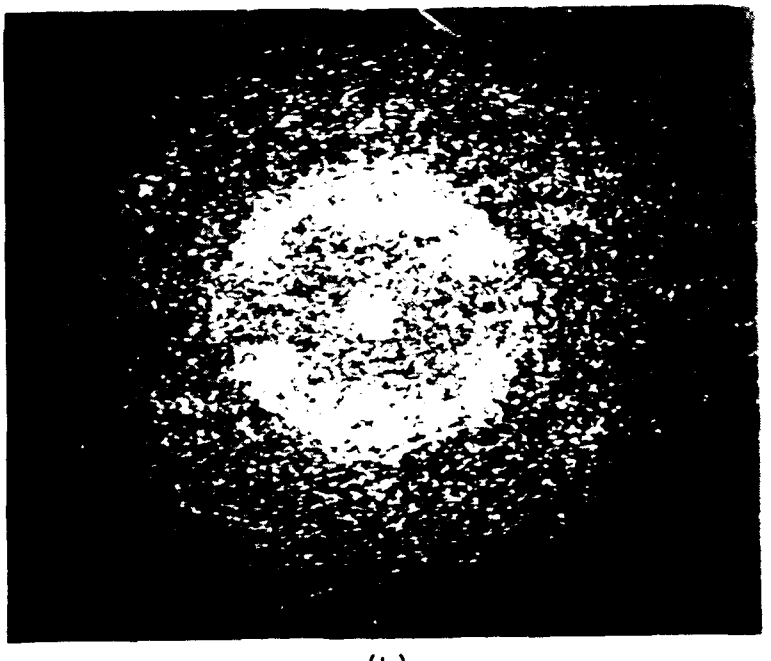

(b)

Figure A-1. Tented Arch Characteristics. (a) A Tented Arch. (b) The Spectrum of the Tented Arch in (a).

(a)

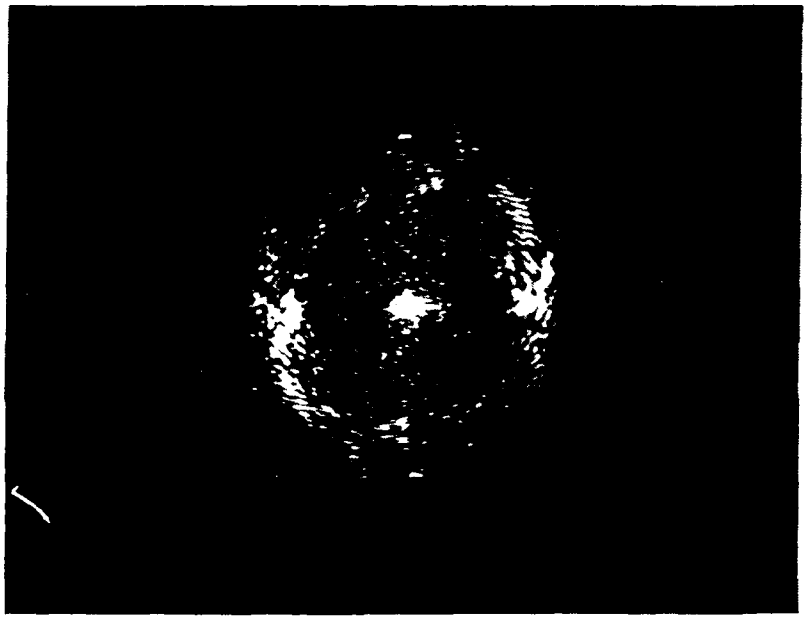

(b)

Figure A-2. Twinned Loop Characteristics. (a) A Twinned Loop. (b) The Spectrum of the Twinned Loop in (a).

(a)

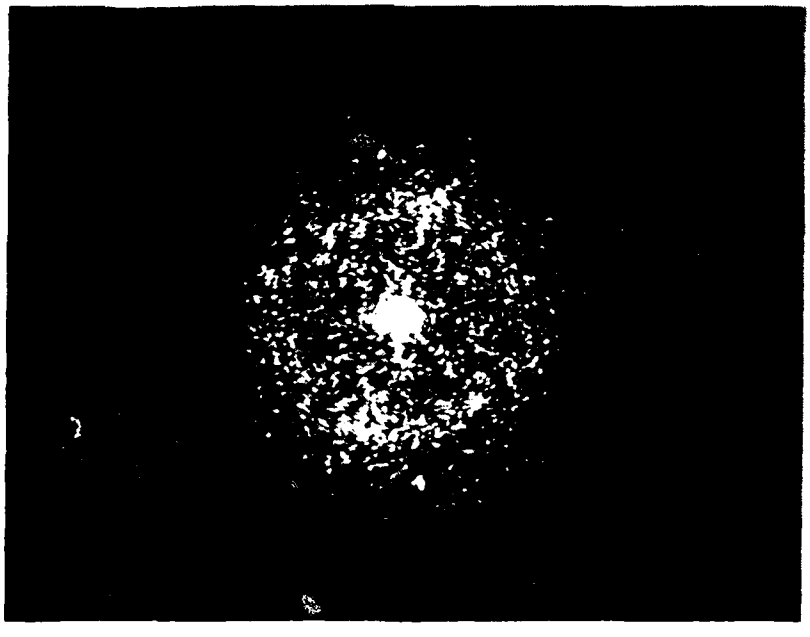

(b)

Figure A-3. Whorl Characteristics. (a) A Whorl.
(b) The Spectrum of the Whorl in (a).

(a)

(b)

Figure A-4. Central Pocket Loop Characteristics. (a) A Central Pocket Loop. (b) The Spectrum of the Central Pocket Loop in (a).

(a)

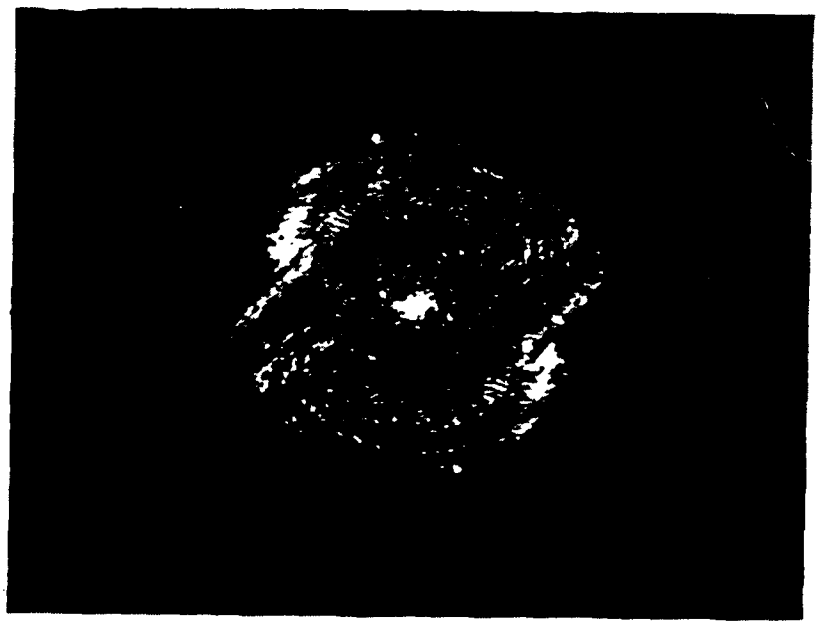

(b)

Figure A-5. Radial Loop Characteristics. (a) A Radial Loop. (b) The Spectrum of the Radial Loop in (a).

END

DTIC

9-86